Goethe Universität Frankfurt

Frankfurt Institute for Advanced Studies

Bachelor thesis

Compact Stars in a Quark-Hadron Model

Pia Jakobus

Supervisor and 1st examiner:

Prof. Stefan Schramm

2nd examiner:

Prof. Armen Sedrakian

November 12, 2017

CONTENTS

1

MOTIVATION

Neutron stars are dense objects that emerge from massive stars larger than $8M_s$ at the end of their stellar evolution. A star that has burned all hydrogen in its core by nucleosynthesis will continue the thermonuclear fusion using heavier elements until only iron is left. The binding energy per nucleon has a maximum at iron. This results in a stagnation of the fusing process, because it would now require instead of release energy to form heavier elements. At that point the hydrostatic equilibrium, and thus the stabilization of the gravitational force due to radiation pressure, ends and the core starts to collapse.
The critical mass for the iron core to become a neutron star is known as Chandrasekhar mass $\mathrm{M}_{ch} = 1.44\ \mathrm{M}_{S}$.
Because the Fermi energy of the dense electrons and protons is higher than the energy necessary to produce the neutron and neutrino with increasing densities during the collapse, electron capture ($p + e^- \rightarrow n + \nu_e$) starts to occur. This causes a rising amount of neutrons inside the star. It is also possible for heavier nucleons than neutrons (and protons) such as the hyperons to appear. These are composed of at least one s quark but no charm- or bottom- quark.
The temporarily trapped neutrinos lead to very high temperatures up to 50 MeV at the inside of the so called proto-neutron stars [30, 8]. In this thesis I will not look at properties of these objects as the temperature inside the star is assumed to be zero in my case.
The moment nuclear density is reached, the Pauli-Blocking leads to a degenerative pressure and prevents the star from further collapsing. When the star finally becomes transparent to neutrinos it starts cooling [30]. Extreme conditions in matter and its consequences like the transition from the hadronic phase to the quark phase are of great interest of many research areas. To find an equation of state (EoS) that appropriately describes this state of matter is linked to many intrinsic properties of QCD. Often times perturbation theory is not applicable due to very high densities and the numerical sign problem prevents Monte Carlo methods in Lattice QCD to give further insights into the properties of quark matter. Heavy ion experiments, where high temperatures and low densities are dominating, and neutron star with low temperatures and high densities are two important research areas that allow access to the properties of the QCD phase diagram. Observations of thermal emission of neutron star are a realistic approach of determining the radius of a neutron star and make it therefore possible to verify physical theories. Figure 1b shows a cartoon of the QCD phase diagram. Figure 1a depicts the important crossover region from the hadron phase to the quark phase

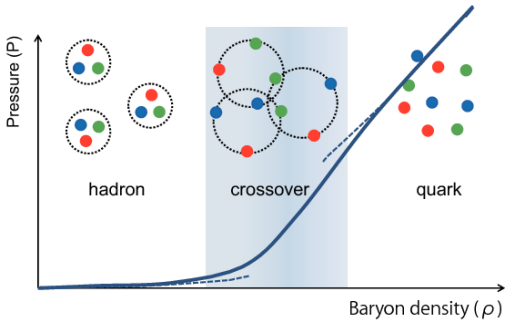

(a) Pressure P as a function of baryon density ρ. One the left side the confined quarks (hadrons) in the hadronic phase. In the middle the crossover region where the hadrons start to overlap on the right side the deconfined quarks which weakly interact.

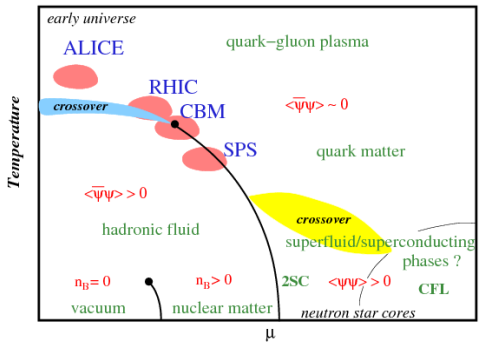

(b) The QCD phase diagram can be divided into three phases. The hadronic, quark gluon plasma and colour superconducting quark matter phase. In the hadronic phase, quarks are confined and appear in form of mesons and baryons. In the deconfined phase, the running coupling constant is small so that the quarks can move approximately free.

Figure 1: QCD phase transition[1]

The theoretical maximum masses and radii of neutron star can be calculated with the Tollman-Oppenheimer-Volkoff equations (TOV-equations). They are two coupled linear differential equations which describe the stellar structure of a star. For an approximation of these properties it is therefore necessary to apply an equation of state, which has been obtained from an appropriate model. In this bachelor thesis I will use different models to obtain equations of state and describe their resulting parameters.

In the second chapter I will give a brief introduction into general relativity.
Concepts like the definition of a metric and the Einstein equation are necessary to derive the TOV-equations. They describe the structure of an isotropic, spherically symmetric object. For lower masses like white dwarfs, the Newtonian formulation of stars is accurate enough since effects arising from the curvature of space-time are negligible small. But for more compact objects like neutron stars gravitational effects must be considered.
Next I will discuss a relativistic and non-relativistic polytropic equation of state for white dwarfs. This is derived from the Fermi gas model of free electrons. The EoS of a free neutron gas will also be shortly discussed. The fourth chapter contains discussion of the Skyrme parametrization, based on a nucleon-nucleon interaction. Also the mass-radius relation will be shown. As a theoretically background for the fourth chapter, chapter five will give a very short introduction to symmetries, the quark model and nuclear field theory.
Following I studied the influences of different parameter of the non-linear-sigma-model to the EoS with a provided program.
In the last section of this thesis, I will explain the structure of my program with an explicit listing of the different implemented modules.

[1] www.inspirehep.net

2

INTRODUCTION TO GENERAL RELATIVITY

General relativity is a theory of gravitation that describes how energy and momentum determine the curvature of spacetime and how in return matter is influenced by curved spacetime. The equations of motion for GR are formulated in a Minkowski four dimensional space. Covariant notation has turned out to be extremely convenient in order to make calculations more comprehensible. In the following the first order derivatives (connection) that is a generalization of partial derivatives in curved spacetime will be introduced as well as the second-order derivative. The Schwarzschild metric, which can be directly derived from the Einstein field equation, is also explained. In the last section I introduce the TOV-equation.

2.1 COVARIANT NOTATION

In special relativity the proper time τ that an observer measures is the same in any frame with constant velocity and the absence of gravity.

$$\mathrm{d}\tau^2 = c^2\mathrm{d}t^2 - \mathrm{d}x^2 - \mathrm{d}y^2 - \mathrm{d}z^2 \tag{1}$$

c is the speed of light, x, y, z and t are the space time coordinates. This is called Lorentz invariance. Lorentz-transformations in general can be shifts in space coordinates, space rotations, time reflection or parity [29].
The so called Minkowski spacetime is the combination of a three dimensional space and the time as a fourth dimension. With the contravariant four-vector $\mathrm{d}x^\mu = \left(x^0, x^1, x^2, x^3\right)$ one can write eq. 1 as

$$\mathrm{d}\tau^2 = \sum_{\mu,\nu=0}^{3} g_{\mu\nu}\mathrm{d}x^\mu\mathrm{d}x^\nu \tag{2}$$

In flat spacetime (and also locally in any other reference frame) the metric tensor is equal to the Minkowski tensor

$$\eta_{\mu\nu} = \begin{pmatrix} 1 & 0 & 0 & 0 \\ 0 & -1 & 0 & 0 \\ 0 & 0 & -1 & 0 \\ 0 & 0 & 0 & -1 \end{pmatrix} \tag{3}$$

$g_{\mu\nu}$ is symmetric, both in its co- and contravariant form

$$g_{\mu\nu} = g_{\nu\mu}, \quad g^{\mu\nu} = g^{\nu\mu}$$

In the following sections I will use the Einstein notation where one sums over repeated indices such that $\sum_{\nu=0}^{3} \mathrm{d}x_\nu\mathrm{d}x^\nu \equiv \mathrm{d}x_\nu\mathrm{d}x^\nu$.

A reference frame is characterized by its state of motion in which an observer is located. The connection between two reference frames $x^\nu \to x'^\nu$ is given by

$$\mathrm{d}x'^\mu = \frac{\partial x'^\mu}{\partial x^\nu}\mathrm{d}x^\nu$$

or for covariant vectors

$$\mathrm{d}x'_\mu = \frac{\partial x^\nu}{\partial x'^\mu}\mathrm{d}x_\nu$$

and a vector which transforms under these Lorentz-transformations the same way as its coordinates is called a contravariant Lorentz-four-vector

$$A'^\mu = \frac{\partial x'^\mu}{\partial x^\nu}A^\nu$$

or covariant Lorentz-four-vector

$$A'_\mu = \frac{\partial x^\nu}{\partial x'^\mu} A^\nu$$

The proper time is invariant under Lorentz-transformations in other words the distance between two space time events is independent of the coordinate systems one chooses.

$$\eta_{\alpha\beta} \mathrm{d}x^\alpha \mathrm{d}x^\beta = g'_{\mu\nu} \mathrm{d}x'^\mu \mathrm{d}x'^\nu$$

one obtains the relation between the Minkowski-tensor (or any other metric tensor) $\eta_{\mu\nu}$ and $g_{\mu\nu}$ by taking the partial derivatives

$$g'_{\mu\nu} = \eta_{\alpha\beta} \frac{\partial x^\alpha}{\partial x'^\mu} \frac{\partial x^\beta}{\partial x'^\nu} \tag{4}$$

2.2 GEODESIC AND AFFINE CONNECTION

The strong equivalence principle states (SEP) that the description of a physical system in a gravitational field is indistinguishable from the description of the same system at rest in an accelerating frame [19]. Put differently, SEP says that in the presence of a gravitational field, no matter how strong, locally one can always find a co-ordinate transformation which 'undoes' the gravitational field. So in other words, an observer, that is free falling in a gravitational field, the results of all local experiments are independent of the magnitude of the gravitational field [17]. The observer is therefore in a local inertial system where the equations of motions (with the coordinates ξ^α of the particle as a function of the basis, coordinates x^μ of the reference frame) can be written as

$$\frac{\mathrm{d}^2 \xi^\alpha}{\mathrm{d}^2 \tau^2} = 0 \tag{5}$$

The equation of motion for an arbitrary reference frame can be derived using the chain rule, product rule and multiplying with $\partial x^\lambda / \partial \xi^\alpha$

$$\begin{aligned}
0 &= \frac{\mathrm{d}}{\mathrm{d}\tau} \left(\frac{\partial \xi^\alpha}{\partial x^\mu} \frac{\mathrm{d}x^\mu}{\mathrm{d}\tau} \right) \\
&= \frac{\partial \xi^\alpha}{\partial x^\mu} \frac{\mathrm{d}^2 x^\mu}{\mathrm{d}^2 \tau^2} + \frac{\partial^2 \xi^\alpha}{\partial x^\mu \partial x^\nu} \frac{\mathrm{d}x^\mu}{\mathrm{d}\tau} \frac{\mathrm{d}x^\nu}{\mathrm{d}\tau} \\
&= \left(\frac{\partial \xi^\alpha}{\partial x^\mu} \frac{\mathrm{d}^2 x^\mu}{\mathrm{d}^2 \tau^2} + \frac{\partial^2 \xi^\alpha}{\partial x^\mu \partial x^\nu} \frac{\mathrm{d}x^\mu}{\mathrm{d}\tau} \frac{\mathrm{d}x^\nu}{\mathrm{d}\tau} \right) \cdot \frac{\partial x^\lambda}{\partial \xi^\alpha} \\
&= \frac{\partial x^\lambda}{\partial \xi^\alpha} \frac{\partial \xi^\alpha}{\partial x^\mu} \frac{\mathrm{d}^2 x^\mu}{\mathrm{d}^2 \tau^2} + \frac{\partial x^\lambda}{\partial \xi^\alpha} \frac{\partial^2 \xi^\alpha}{\partial x^\mu \partial x^\nu} \frac{\mathrm{d}x^\mu}{\mathrm{d}\tau} \frac{\mathrm{d}x^\nu}{\mathrm{d}\tau} \\
&= \frac{\mathrm{d}^2 x^\lambda}{\mathrm{d}^2 \tau^2} + \frac{\partial x^\lambda}{\partial \xi^\alpha} \frac{\partial^2 \xi^\alpha}{\partial x^\mu \partial x^\nu} \frac{\mathrm{d}x^\mu}{\mathrm{d}\tau} \frac{\mathrm{d}x^\nu}{\mathrm{d}\tau} \\
\Leftrightarrow 0 &= \frac{\mathrm{d}^2 x^\lambda}{\mathrm{d}^2 \tau^2} + \Gamma^\lambda_{\mu\nu} \frac{\mathrm{d}x^\mu}{\mathrm{d}\tau} \frac{\mathrm{d}x^\nu}{\mathrm{d}\tau}
\end{aligned} \tag{6}$$

where $\frac{\partial x^\lambda}{\partial \xi^\alpha} \frac{\partial \xi^\alpha}{\partial x^\mu} = \frac{\mathrm{d}x^\lambda}{\mathrm{d}x^\mu} = \delta^\lambda_\mu$ and

$$\Gamma^\lambda_{\mu\nu} = \frac{\partial x^\lambda}{\partial \xi^\alpha} \frac{\partial^2 \xi^\alpha}{\partial x^\mu \partial x^\nu} \tag{7}$$

is the affine connection which is symmetric in its lower indices.
Eq. 6 is called a geodesic equation. A geodesic is the extremal path of a particle in spacetime i.e. the shortest-distance path between two points in spacetime. This turns out to be the curve of a maximum proper time $\mathrm{d}s$ [5]. The affine connection in flat space vanishes in Cartesian coordinates (so that the affine connection is just equivalent to eq. 5) but does not vanish in a flat space space with polar coordinates. So generally speaking,

for arbitrary non local reference frames $\Gamma^{\lambda}_{\mu\nu}$ does not vanish.
A mathematical problem is that the affine connection does not transform like a tensor [15].
This is why one takes the derivative of $(\partial/\partial x'^{\kappa})g'_{\mu\nu}$ and uses the product rule and eq. 4. The result is a second non-tensor $\{^{\lambda}_{\mu\nu}\}$ which transforms exactly the same way as the affine connection so that the difference transforms as

$$\left[\Gamma^{\lambda}_{\mu\nu} - \{^{\lambda}_{\mu\nu}\}\right]' = \frac{\partial x'^{\lambda}}{\partial x^{\rho}} \frac{\partial x^{\tau}}{\partial x'^{\mu}} \frac{\partial x^{\sigma}}{\partial x'^{\nu}} \left[\Gamma^{\rho}_{\tau\sigma} - \{^{\rho}_{\tau\sigma}\}\right] \tag{8}$$

and is therefore a tensor.
$\{^{\lambda}_{\mu\nu}\}$ is called Christoffel symbol of the second kind

$$\{^{\lambda}_{\mu\nu}\} = \frac{1}{2} g^{\lambda\kappa} \left(g_{\kappa\nu,\mu} + g_{\kappa\mu,\nu} + g_{\mu\nu,\kappa}\right) \tag{9}$$

with $\partial g_{\kappa\nu}/\partial x^{\mu} = g_{\kappa\nu,\mu}$. Its derivation is easy after introducing the covariant derivative of the metric tensor and the metric compatibility (eq. 18) and 19 but not shown in here. A derivation can be found here [5]. A formulation of the equivalence principle is that in the local region around an event P the metric tensor, the the coordinate derivative and the affine connection have the values

$$g_{\mu\nu}(P) = n_{\mu\nu} \tag{10}$$

$$g_{\mu\nu,\alpha}(P) = 0 \tag{11}$$

$$\Gamma^{\lambda}_{\mu\nu}(P) = 0 \tag{12}$$

This is an equivalent, more mathematically formulation of the equivalence principle as it was described in the beginning of this section. Any small region around a point P in the four-dimensional space can be described with the metric tensor $g_{\mu\nu}(P) = n_{\mu\nu}$ so that for all partial derivatives $g_{\mu\nu,\alpha}(P) = 0$ (second bullet point). With eq. 9 one sees that the third bullet point is a consequence of the first one

$$\Gamma^{\lambda}_{\mu\nu}(P) = 0$$

As the partial derivatives of the metric tensor $g_{\mu\nu}$ vanish, so do the Christoffel symbols (eq. 9) Therefore the difference of Christoffel symbols and affine connection vanishes as well (eq. 8). The difference transforms as a tensor so that it becomes zero in any other arbitrary reference frames (under the assumption that there is no torsion)

$$\Gamma^{\lambda}_{\mu\nu} = \{^{\lambda}_{\mu\nu}\} = \frac{1}{2} g^{\lambda\kappa} \left(g_{\kappa\nu,\mu} + g_{\kappa\mu,\nu} + g_{\mu\nu,\kappa}\right) \tag{13}$$

In summary: In an arbitrary gravitational field, at any given spacetime point, we can choose a locally inertial reference frame such that in a sufficiently small region surrounding that point all physical laws take the same form they would take in absence of gravity, namely the form prescribed by Special Relativity.

2.3 COVARIANT DERIVATIVE OF VECTORS AND THE METRIC TENSOR

Covariant derivatives generalize differentiation of vector fields for arbitrary spaces. The Problem with 'normal' derivatives is (as we know it from Euclidean space like e.g. $\frac{\mathrm{d}u}{\mathrm{d}t}$) that the space itself can have an arbitrary curvature. Let's look at the interval $u(P_1) - u(P_2)$. If the spacetime 'points' P_1 and P_2 belong to different bases in vector spaces of $\mathbb{R}^4$, the concept of distance becomes invalid because the unit of distance itself changes. A more mathematically formulation of this problem is that normal derivatives of vectors do not transform like tensors. But the central aspect of general relativity is that arbitrary systems can be regarded as inertial frames which are well-defined in an infinitesimal neighbourhood of a spacetime point. Thus tensor transformations between arbitrary reference frames must always be possible to ensure generally valid physical laws independent of their (local) inertial reference frame [40].

2.3.1 *First order derivative*

The derivative of scalars can be written as

$$\frac{\partial S}{\partial x^\mu} = S_{,\mu}$$

this is a vector with transformation properties

$$\frac{\partial S}{\partial x'^\mu} = \frac{\partial x^\nu}{\partial x'^\mu}\frac{\partial S}{\partial x^\nu}$$

which shows, that it transforms as a covariant vector. One can also take the derivative of a vector (equation 2.1), the result however is an expression which does not transform like a tensor:

$$\frac{\mathrm{d}A'_\mu}{\mathrm{d}x'^\rho} = \frac{\partial x'^\nu}{\partial x'^\mu}\frac{\partial x^\sigma}{\partial x'^\rho}\frac{\partial A_\nu}{\partial x^\sigma} + \frac{\partial^2 x^\nu}{\partial x'^\rho \partial x'^\mu}A_\nu \tag{14}$$

It is therefore necessary to introduce the so called co-variant derivative which does transform like a vector.

$$A_{\mu;\nu} \equiv \frac{\partial A_\mu}{\partial x^\nu} - \Gamma^\lambda_{\mu\nu}A_\lambda \tag{15}$$

covariant derivatives of a contravariant vector are defined as

$$A^\mu_{;\nu} \equiv \frac{\partial A^\mu}{\partial x^\nu} - \Gamma^\mu_{\sigma\nu}A_\sigma \tag{16}$$

Both are second rank, mixed tensors and therefore of course transform like a tensor as can be easily seen:

$$\frac{\partial A'_\mu}{\partial x'^\nu} - \Gamma'^\lambda_{\mu\nu}A'_\lambda = \frac{\partial x^\alpha}{\partial x'^\mu}\frac{\partial x^\beta}{\partial x'^\nu}\left(\frac{\partial A_\alpha}{\partial x^\beta} - \Gamma^\lambda_{\alpha\beta}A_\lambda\right) \tag{17}$$

The covariant derivative of the metric tensor can be calculated as

$$g_{\mu\nu;\lambda} = \frac{\partial g_{\mu\nu}}{\partial x^\lambda} - \Gamma^\rho_{\mu\lambda}g_{\rho\nu} - \Gamma^\rho_{\nu\lambda}g_{\rho\mu} \tag{18}$$

As previously shown, the derivatives of the metric tensor vanish in a local inertial frame and so do the Christoffel symbols. Looking at eq. 18 it becomes obvious that also the covariant derivative of $g^{\mu\nu}$ vanishes. It itself is a tensor hence it vanishes in all frames. This is called metric compatibility

$$g_{\mu\nu;\lambda} = g^{\mu\nu;\lambda} = 0 \tag{19}$$

Metric compatibility simplifies covariant derivatives because it commutes with raising and lowering indices. By example

$$g_{\mu\nu}V^\nu_{;\lambda} = (g_{\mu\nu}V^\nu)_{;\lambda} = V_{\mu;\lambda} \tag{20}$$

is a nice property as one can contract indices by shifting the metric tensor into the brackets. With non-metric compatible connections (a connection is metric compatible if the covariant derivative of the metric with respect to that connection is everywhere zero [5]), one has to be very careful about index placement.

2.3.2 *Second order derivative*

In curved spacetime, the order of covariant differentiation matters while the order of covariant differentiation of a scalar does not. This can easily be verified by looking at the difference $S_{;\mu;\nu} - S_{;\nu;\mu}$

$$\begin{aligned} S_{;\mu;\nu} - S_{;\nu;\mu} &= S_{,\mu;\nu} - S_{;\nu\mu} = (\partial_\nu S)_{;\mu} - (\partial_\mu S)_{;\nu} \\ &= \partial_\mu\partial_\nu S - \Gamma^\lambda_{\mu\nu}\partial_\lambda S - \partial_\nu\partial_\mu S + \Gamma^\lambda_{\nu\mu}\partial_\lambda S \qquad (21)\\ &= 0 \qquad (22)\\ &\Rightarrow S_{;\mu;\nu} = S_{;\nu\mu} \qquad (23) \end{aligned}$$

I used twice that the covariant derivative is the same as the ordinary derivative $S_{;\mu} = S_{,\mu}$. The Christoffel symbols are symmetric in their lower indices and the normal differentiation in flat spacetime is independent of its order so that the right side of eq. 21 is also symmetric in μ and ν. Therefore the order of covariant differentiation does not matter for scalars.
For vectors this does not hold. Their second derivative can be calculated with the so called Riemann tensor $R^{\rho}_{\sigma\mu\nu}$

$$A_{\sigma;\mu;\nu} - A_{\sigma;\nu;\mu} = A_{\rho} R^{\rho}_{\sigma\mu\nu}, \tag{24}$$

where

$$R^{\rho}_{\sigma\mu\nu} \equiv \Gamma^{\rho}_{\sigma\nu,\mu} - \Gamma^{\rho}_{\sigma\mu,\nu} + \Gamma^{\alpha}_{\sigma\nu}\Gamma^{\rho}_{\alpha\mu} - \Gamma^{\alpha}_{\sigma\mu}\Gamma^{\rho}_{\alpha\nu} \tag{25}$$

is constrained only by the derivatives of the metric tensor and therefore a measure for the curvature of the space time. It will vanish if the metric is perfectly flat. Some important properties which will also be used later are

$$0 = R^{\alpha}_{\nu\rho\sigma} + R^{\alpha}_{\sigma\nu\rho} + R^{\alpha}_{\rho\sigma\nu} \tag{26}$$

$$R^{\mu}_{\nu\rho\sigma} = -R^{\mu}_{\nu\sigma\rho} \tag{27}$$

$$R_{\mu\nu\rho\sigma} = -R_{\nu\mu\rho\sigma} = R_{\nu\mu\sigma\rho} \tag{28}$$

The Ricci tensor is defined as

$$R_{\mu\nu} = R^{\rho}_{\mu\nu\rho} \tag{29}$$

and the scalar curvature reads

$$R = g^{\mu\nu} R_{\mu\nu} \tag{30}$$

Now for taking the second derivative of a tensor, it is useful to set an arbitrary second rank tensor as the product of two covariant vectors $T_{\mu\nu} \equiv A_{\mu} B_{\nu}$.

$$\begin{aligned}(A_{\mu}B_{\nu})_{;\rho;\sigma} &= (A_{\mu;\rho}B_{\nu} + A_{\mu}B_{\nu;\rho})_{;\sigma} \\ &= A_{\mu;\rho;\sigma}B_{\nu} + A_{\mu}B_{\nu;\rho;\sigma} + A_{\mu;\rho}B_{\nu;\sigma} + A_{\mu;\sigma}B_{\nu;\rho}\end{aligned}$$

Now one substracts this expression with flipped indices $(A_{\mu}B_{\nu})_{;\sigma;\rho}$

$$\begin{aligned}&(A_{\mu}B_{\nu})_{;\rho;\sigma} - (A_{\mu}B_{\nu})_{;\sigma;\rho} \\ &= A_{\mu;\rho;\sigma}B_{\nu} + A_{\mu}B_{\nu;\rho;\sigma} + A_{\mu;\rho}B_{\nu;\sigma} + A_{\mu;\sigma}B_{\nu;\rho} \\ &- (A_{\mu;\sigma;\rho}B_{\nu} + A_{\mu}B_{\nu;\sigma;\rho} + A_{\mu;\sigma}B_{\nu;\rho} + A_{\mu;\rho}B_{\nu;\sigma}) \\ &= A_{\mu}(B_{\nu;\rho;\sigma} - B_{\nu;\sigma;\rho}) + (A_{\mu;\rho;\sigma} - A_{\mu;\sigma;\rho}B_{\nu}) \\ &= A_{\mu}B_{\alpha}R^{\alpha}_{\nu\rho\sigma} + A_{\alpha}R^{\alpha}_{\mu\rho\sigma}B_{\nu}\end{aligned}$$

Since one can take any linear combination of first rank tensors, the general form for a tensor takes the following form:

$$T_{\mu\nu;\rho;\sigma} - T_{\mu\nu;\sigma;\rho} = T_{\mu\alpha}R^{\alpha}_{\nu\rho\sigma} + T_{\alpha\nu}R^{\alpha}_{\mu\rho\sigma} \tag{31}$$

2.4 BIANCHI IDENTITIES AND EINSTEIN TENSOR

The Bianchi identities result from second derivative of a tensor. With eq. 31 we set $T_{\mu\nu} = A_{\mu;\nu}$ with $T_{\mu\nu}$ as an arbitrary second rank tensor.

$$A_{\mu;\nu;\rho;\sigma} - A_{\mu;\nu;\sigma;\rho} = A_{\mu;\alpha}R^{\alpha}_{\nu\rho\sigma} + A_{\alpha;\nu}R^{\alpha}_{\mu\rho\sigma} \tag{32}$$

Now one sums up all cyclic permutations of the order of the derivatives $;\mu,;\nu,;\sigma$ (see eq. 31). Th left side then reads

$$\begin{aligned}&(A_{\mu;\nu;\rho;\sigma} - A_{\mu;\nu;\sigma;\rho}) + (A_{\mu;\sigma;\nu;\rho} - A_{\mu;\rho;\nu;\sigma}) + (A_{\mu;\rho;\sigma;\nu} - A_{\mu;\sigma;\rho;\nu}) \\ &= (A_{\mu;\nu;\rho} - A_{\mu;\rho;\nu})_{;\sigma} + (A_{\mu;\sigma;\nu} - A_{\mu;\nu;\sigma})_{;\rho} + (A_{\mu;\rho;\sigma} - A_{\mu;\sigma;\rho})_{;\nu} \\ &= (A_{\alpha}R^{\alpha}_{\mu\nu\rho})_{;\sigma} + (A_{\alpha}R^{\alpha}_{\mu\sigma\nu})_{;\rho} + (A_{\alpha}R^{\alpha}_{\mu\rho\sigma})_{;\nu}\end{aligned}$$

We evaluate the right side of eq. 32

$$\begin{aligned} &A_{\mu;\alpha}R^{\alpha}_{\nu\rho\sigma} + A_{\alpha;\nu}R^{\alpha}_{\mu\rho\sigma} + A_{\mu;\alpha}R^{\alpha}_{\sigma\nu\rho} + A_{\alpha;\sigma}R^{\alpha}_{\mu\nu\rho} + A_{\mu;\alpha}R^{\alpha}_{\rho\sigma\nu} + A_{\alpha;\rho}R^{\alpha}_{\mu\sigma\nu} \\ &= A_{\mu;\alpha}(R^{\alpha}_{\nu\rho\sigma} + R^{\alpha}_{\sigma\nu\rho} + R^{\alpha}_{\rho\sigma\nu}) + A_{\alpha;\nu}R^{\alpha}_{\mu\rho\sigma} + A_{\alpha;\sigma}R^{\alpha}_{\mu\nu\rho} + A_{\alpha;\rho}R^{\alpha}_{\mu\sigma\nu} \end{aligned}$$

With the property of the Riemann tensor (eq. 26), the first term vanishes. Equating left and right hand side leads to

$$\begin{aligned} &(A_\alpha R^{\alpha}_{\mu\nu\rho})_{;\sigma} + (A_\alpha R^{\alpha}_{\mu\sigma\nu})_{;\rho} + (A_\alpha R^{\alpha}_{\mu\rho\sigma})_{;\nu} = A_{\alpha;\nu}R^{\alpha}_{\mu\rho\sigma} + A_{\alpha;\sigma}R^{\alpha}_{\mu\nu\rho} + A_{\alpha;\rho}R^{\alpha}_{\mu\sigma\nu} \\ &\leftrightarrow \cancel{A_{\alpha;\sigma}R^{\alpha}_{\mu\nu\rho}} + A_\alpha R^{\alpha}_{\mu\nu\rho;\sigma} + \cancel{A_{\alpha;\rho}R^{\alpha}_{\mu\sigma\nu}} + A_\alpha R^{\alpha}_{\mu\sigma\nu;\rho} + \cancel{A_{\alpha;\nu}R^{\alpha}_{\mu\rho\sigma}} + A_\alpha R^{\alpha}_{\mu\rho\sigma;\nu} \\ &= \cancel{A_{\alpha;\nu}R^{\alpha}_{\mu\rho\sigma}} + \cancel{A_{\alpha;\sigma}R^{\alpha}_{\mu\nu\rho}} + \cancel{A_{\alpha;\rho}R^{\alpha}_{\mu\sigma\nu}} \end{aligned}$$

The remaining terms form the bianchi identities

$$A_\alpha(R^{\alpha}_{\mu\nu\rho;\sigma} + R^{\alpha}_{\mu\sigma\nu;\rho} + R^{\alpha}_{\mu\rho\sigma;\nu}) = 0 \leftrightarrow R^{\alpha}_{\mu\nu\rho;\sigma} + R^{\alpha}_{\mu\sigma\nu;\rho} + R^{\alpha}_{\mu\rho\sigma;\nu} = 0 \tag{33}$$

A_α is an arbitrary first rank tensor.
With all the expressions obtained so far, it is now possible to write down the Einstein equation. I will not show each step, details are found here [15]. In summary, one multiplies the Bianchi identity twice with the metric tensor $g_{\mu\nu}$ and $g^{\mu\rho}$

$$\begin{aligned} 0 &= g^{\mu\nu}\left(R^{\alpha}_{\mu\nu\rho;\sigma} + R^{\alpha}_{\mu\sigma\nu;\rho} + R^{\alpha}_{\mu\rho\sigma;\nu}\right) \\ &= 2R^{\alpha}_{\rho;\alpha} - R_{;\nu} \\ &= g^{\mu\rho}(2R^{\alpha}_{\rho;\alpha} - R_{;\nu}) \end{aligned}$$

and then uses the properties of the Riemann and Ricci tensor and does some renaming and contracting indices transformations.

$$\left(R^{\mu\nu} - \frac{1}{2}g^{\mu\nu}R\right)_{;\nu} = 0 \tag{34}$$

$G_{\mu\nu} = R^{\mu\nu} - \frac{1}{2}g^{\mu\nu}R$ is the Einstein tensor and shortens the equation to

$$G_{\mu\nu;\,\nu} = 0 \tag{35}$$

The divergence of this second rank tensor is zero as it also is the case for the stress energy tensor. One equates the Einstein tensor with the energy stress tensor which divergence is also zero times a proportionality constant $\kappa = -8\pi G$, with G as the gravitational constant. $T^{\mu\nu}$ is a second rank, symmetric tensor. The Einstein field equations then read

$$G^{\mu\nu} = -8\pi G T^{\mu\nu} \tag{36}$$

This equation is a set of 10 non-linear partial differential equations containing derivatives of the metric tensor $g_{\mu\nu}$ which one wants to solve. Because the tensor is symmetric the upper and lower half of it are identical. Due to its covariant form, the Einstein equations are invariant of the chosen coordinate system. Of course the solutions for $g_{\mu\nu}$ in another basis will look different and it can be useful for simplifying calculations to choose a well-considered one but it is possible to transform between those bases.
Regarding eq. 36, there can also exist (due to the vanishing derivative of the metric tensor) more solutions like

$$-8\pi G T^{\mu\nu} - \Lambda g^{\mu\nu} \tag{37}$$

$\Lambda g^{\mu\nu}$ is called cosmological term. Its sign and size in different phases of development of the universe have a huge impact on the expanding or delayed expansion of it. Further information about this can be found here [14]. An alternative way to derive the Einstein equations is the principle of least action, called Einstein-Hilbert action [2].

$$S = \frac{1}{2\kappa}\int R\sqrt{-g}\,\mathrm{d}^4x$$

With the variables as defines and g being the determinant of the metric tensor. The general form with matter field appearing is

$$S = \frac{1}{2\kappa}\int \left[R + \mathcal{L}_M\right]\sqrt{-g}\,\mathrm{d}^4x$$

2.5 SCHWARZSCHILD METRIC

In this section I will give a brief overview over the derivation of the Schwarzschild metric. This metric can be divided into two parts, the inner solution, which describes the metric inside a star or any mass distribution, and the outer solution, for outside a massive object. There are two assumptions to be made [11]:

- static solution: the components of the metric tensor are all time independent and there exists no space-time mix term
- spheric solution: the mass is supposed to be spherically symmetric

The first step will be deriving the scalar curvature. Then one can distinguish the two cases outside a star (Einstein tensor is zero) and inside (non vanishing Einstein tensor).
In a curved isotropic spherical space time with a zero time component the line element is of the form

$$\mathrm{d}s^2 = e^{2\alpha(r)}\mathrm{d}t^2 - e^{2\beta(r)}\mathrm{d}r^2 - r^2\mathrm{d}\theta^2 - r^2\sin^2\theta\mathrm{d}\phi^2 \tag{38}$$

Exponential pre-factors have been chosen to make sure that one obtains the signature of the metric [11]. The metric tensor in its general form for the Schwarzschild metric looks like this:

$$g_{\mu\nu} = \begin{pmatrix} e^{2\alpha(r)} & 0 & 0 & 0 \\ 0 & -e^{2\beta(r)} & 0 & 0 \\ 0 & 0 & -r^2 & 0 \\ 0 & 0 & 0 & -r^2\sin^2\theta \end{pmatrix} \tag{39}$$

$$g^{\mu\nu} = \begin{pmatrix} e^{-2\alpha(r)} & 0 & 0 & 0 \\ 0 & -e^{-2\beta(r)} & 0 & 0 \\ 0 & 0 & -\frac{1}{r^2} & 0 \\ 0 & 0 & 0 & -\frac{1}{r^2\sin^2\theta} \end{pmatrix} \tag{40}$$

For arbitrary metrics the off diagonals do not need to be zero thus the invertation of the matrix $g^{\mu\nu}$ can be more complicated. It is now possible to derive the Schwarzschild solution in a few steps. I will give an overview over the procedure for the derivation without going into much detail. The exact derivation can be found here [12].
The line element for an isotropic spherical space time (eq. 38) has two functions ($\alpha(r)$ and $\beta(r)$) that need to be determined. The first step to obtain them is calculating the components of the Christoffel symbols. This is done by taking the derivatives of the metric tensor (eq. 25).

$$\left\{{}^{\lambda}_{\mu\nu}\right\} \equiv \frac{1}{2}g^{\lambda\kappa}\left(g_{\kappa\nu,\mu} + g_{\kappa\mu,\nu} + g_{\mu\nu,\kappa}\right) \tag{41}$$

With the Christoffel symbols, one can derive the Riemann-Christoffel-curvature tensor

$$R^{\rho}_{\sigma\mu\nu} \equiv \Gamma^{\rho}_{\sigma\nu,\mu} - \Gamma^{\rho}_{\sigma\mu,\nu} + \Gamma^{\alpha}_{\sigma\nu}\Gamma^{\rho}_{\alpha\mu} - \Gamma^{\alpha}_{\sigma\mu}\Gamma^{\rho}_{\alpha\nu} \tag{42}$$

From here one can derive the Ricci tensor with eq. 29. Its non vanishing components are

$$R_{00} = \left(-\alpha'' + \beta'\alpha' - \alpha'^2 - \frac{2\alpha'}{r}\right)e^{\alpha-\beta} \tag{43}$$

$$R_{11} = \alpha'' - \beta'\alpha' + \alpha'^2 - \frac{2\beta'}{r} \tag{44}$$

$$R_{22} = \left(1 + r\alpha' - r\beta'\right)e^{-2\beta} - 1 \tag{45}$$

$$R_{33} = R_{22}\sin^2\theta \tag{46}$$

As mentioned, α and β are the pre-factor of the two first terms for the line element $\mathrm{d}s^2$, α', β' and their derivatives with respect to r. The scalar curvature $R = g^{\mu\nu}R_{\mu\nu}$ then reads

$$R = e^{-2\alpha}R_{00} - e^{-2\beta}R_{11} - \frac{2}{r^2}R_{22} \tag{47}$$

2.6 OUTER SCHWARZSCHILD SOLUTION

Because of $T^{\mu\nu} = 0$ outside a star, the Einstein tensor $G^{\mu\nu}$ outside a star vanishes (see eq. 36). Multiplying $R^{\mu\nu} - \frac{1}{2}g^{\mu\nu}R = 0$ with $g_{\mu\nu}$ yields $R = \frac{1}{2}R$ and therefore $R = 0 \rightarrow R^{\mu\nu} = 0$ (eq. 30) for a non vanishing metric tensor, more details here [12].
With the Ricci tensor and the scalar curvature both vanishing, the next step is to solve eq. 43 to 47 for α and β and then evaluating the pre-factors of eq. 38. This leads to the line element for the outer Schwarzschild solution. The components read

$$e^{2\beta} = e^{-2\alpha} = \left(1 - \frac{2GM}{r}\right) \tag{48}$$

with M identified as the mass of the star and for $r > R$. It derives from an integration constants and the Newtonian limit [24].. The line element reads

$$\mathrm{d}s^2 = \left(1 - \frac{2GM}{r}\right)\mathrm{d}t^2 - \left(1 - \frac{2GM}{r}\right)^{-1}\mathrm{d}r^2 \tag{49}$$

$$- r^2\mathrm{d}\theta^2 - r^2\sin^2\theta\mathrm{d}\phi^2 \tag{50}$$

with the metric tensor given by

$$g_{\mu\nu} = \begin{pmatrix} \left(1 - \frac{2GM}{r}\right) & 0 & 0 & 0 \\ 0 & -\left(1 - \frac{2GM}{r}\right)^{-1} & 0 & 0 \\ 0 & 0 & -r^2 & 0 \\ 0 & 0 & 0 & -r^2\sin^{\theta} \end{pmatrix}$$

2.7 TOLMAN-OPPENHEIMER-VOLKOFF EQUATION

For the TOV-equation, one solves the Einstein equation with a non vanishing right side of the Ricci tensor and scalar curvature (because one looks at the interior of the star, the energy momentum tensor obviously does not vanish)

$$8\pi G T^{\mu\nu} = \left(R^{\mu\nu} - \frac{1}{2}g^{\mu\nu}R\right) \tag{51}$$

The energy momentum tensor for a perfect fluid has the form

$$T^{\mu\nu} = \begin{pmatrix} \epsilon & 0 & 0 & 0 \\ 0 & -p & 0 & 0 \\ 0 & 0 & -p & 0 \\ 0 & 0 & 0 & -p \end{pmatrix}$$

With the components of the Ricci Tensor (eq. 43-46) and the curvature (eq. 47) it is now possible to derive the TOV equations by inserting the components in the field equations (eq. 51) in the same way as for the outer Schwarzschild solution. At the surface of the star the solution has to converge into the outer Schwarzschild solution. I will not give a derivation of the TOV equation and just write down the solution, for a detailed derivation see here [15].

$$\frac{\mathrm{d}P}{\mathrm{d}r} = -\frac{G\epsilon\,(r)\,m\,(r)}{c^2r^2}\left[1 + \frac{p\,(r)}{\epsilon\,(r)}\right]\left[1 + \frac{4\pi r^3 p\,(r)}{m\,(r)\,c^2}\right]\left[1 - \frac{2Gm\,(r)}{rc^2}\right]^{-1} \tag{52}$$

The TOV equation is a central equation in this thesis as in the following chapters maximum masses and radii of different EoS will be discussed, which is done by solving the TOV equation. In the non relativistic limit $c \rightarrow \infty$, the relativistic corrections vanish and one obtains the Newtonian formulation (derivation see appendix)[42] .

$$\frac{\mathrm{d}p}{\mathrm{d}r} = -\frac{G\pi\epsilon(r)m(r)}{c^2r^2}$$

3

POLYTROPIC EOS

Low or medium mass stars ($< 8M_S$) that do not thermonuclearly burn up to iron (due to their lower masses compared to neutron stars) like it is the case with our sun, end as a white dwarf. These objects are also extreme dense (e.g. a typical white dwarf with one solar mass would have the radius of the earth) and in contrast to neutron stars also very hot. One can approximate the matter of a white dwarf as a free electron gas. The first section in this chapter contains the derivation of two so called Polytropic EoS. The first case is the non relativistic one with $k_F \ll m_e$ (i.e. the kinetic energy of the electrons is much smaller than their rest mass). The second one is the relativistic case, with $k_F \gg m_e$ (i.e. high kinetic energy of the electrons).

3.1 FERMI GAS MODEL FOR FREE ELECTRONS

The Pauli exclusion principle, which is equivalent to the requirement of a total antisymmetric wave function for fermions forces fermionic particles not to be in the same quantum state at energy E_i. If all energy states up to the Fermi-energy are occupied and the thermal energy is much smaller than the Fermi-energy ($k_B T \ll E_F \Leftrightarrow \frac{E_F}{k_B T} \gg 1$) then one refers to degenerate matter. This means that the Fermi-pressure prevents the star from collapsing as a result of the gravitational force.
An electron with energy E_i can either have spin up, $|\frac{1}{2}\rangle$ or spin down, $|-\frac{1}{2}\rangle$ (while all other quantum numbers are identical), so that there is a maximum occupation of two electrons per energy state. This case is called degeneracy of E_i. For electrons the degeneracy is two.
The probability distribution of a fermion to be located at a state $|i\rangle$ with energy E_i is given by the Fermi-Dirac distribution.

$$f(E_i) = \frac{1}{\exp\left(\frac{E_i - \mu}{k_B T}\right) + 1} \tag{53}$$

E_i is the energy of a fermion at state $|i\rangle$, μ is the chemical potential and $k_B T$ the thermal energy. The number of particles inside an energy interval $\mathrm{d}\epsilon$ is given by

$$\mathrm{d}N = g \cdot n(\epsilon) f(\epsilon) \mathrm{d}\epsilon, \tag{54}$$

where $n(\epsilon)$ is the density of states and $g = 2$ for fermions. The density of states describes the number of states in the interval $\mathrm{d}\epsilon$ at an energy level ϵ.
In k-space (the reciprocal space), where $k = \hbar p$ is the wave vector, the density of states is given by

$$\mathrm{d}n = 2 \cdot f(k) \cdot \frac{\mathrm{d}^3 k}{(2\pi\hbar)^3} \tag{55}$$

we now sum over all momentum states k inside the unit volume. The unit volume $(2\pi\hbar)^3$ comes from the integral measure during the transformation of the sum $\sum_{\mathbf{k}} ... \rightarrow \int_0^\infty \frac{\mathrm{d}^3 k}{(2\pi\hbar)^3} ...$ into an integral. As mentioned before, at high pressures or low temperature, states up to the Fermi-energy states can't be filled with more particles because they are already occupied. The approximated probability for a particle of degenerate matter to be at state $|i\rangle$ in this case is

$$f(k) = \Theta(k - k_0)$$

with $k_F = \frac{\sqrt{2m_e E_F}}{\hbar}$.
By integrating over phase space, equation 55 yields the number density of a degenerate electron gas

$$n = \int_0^{k_F} \frac{1}{4(\pi\hbar)^3} \mathrm{d}^3k \tag{56}$$

$$= \frac{1}{\pi^2\hbar^3} \int_0^{k_F} k^2 \mathrm{d}^3k \tag{57}$$

$$= \frac{k_F^3}{3\pi^2\hbar^3} \tag{58}$$

So for degenerate matter, n gives the number of particles with a momentum $0 \leq k \leq k_F$ inside the unit volume.
In the following I will derive an equation for the energy density ϵ as a function of k_F. From there one can derive the relation $p(k_F)$ via thermodynamic relations. We distinguish between high kinetic energy of the electrons where $k_F \gg m_e$ and the low energy, non relativistic case where $k_F \ll m_e$. This results in an approximation $p(\epsilon)$ under the assumption that the energy-density is dominated by the mass of the nucleons. Because white dwarf matter is charge neutral, each electron is accompanied by one proton (mass number Z) and a number of neutrons. Assuming this, the number of nucleons per electron is given by $\frac{A}{Z}$, where A is the sum of neutron and protons. For star matter which is predominately ^{12}C, this ratio is 2. As the electron rest mass is much smaller than the masses of the nucleons, it will be neglected in a first approximation. ρ, the mass density of the nucleons, can then be written as

$$\rho_{star} = n \cdot m_N \cdot \frac{A}{Z} \tag{59}$$

with the nucleon mass m_N and n the number of electrons which was set equal to the number of protons. Solving ρ_{star} for n and equating with eq. 56 leads to

$$k_F = \hbar \left(\frac{3\pi^2 \rho Z}{m_N A} \right)^{1/3} \tag{60}$$

For the next step one calculates the energy density $\epsilon(k_F)$ and deriving $p(k_F)$ via thermodynamic relations.
The energy density can be split into two parts

$$\epsilon = \rho_{nucl} c^2 + \epsilon_{elec}(k_F) \tag{61}$$

where the first term is the nucleon mass of the star and the latter is the energy-density contribution of the electrons which also includes their rest mass. I will now derive the second term.
For brevity one sets $\hbar = 1$ which results in energy and mass units being equivalent. Using eq. 56 with the relativistic energy momentum relation $m^2c^4 = E^2 - p^2c^2$ (the momentum can be identified with the k-vector: $\mathbf{p} = \hbar\mathbf{k}$) yields

$$\epsilon_{elec}(k_F) = \frac{1}{\pi^2\hbar^3} \int_0^{k_F} E(k) k^2 \mathrm{d}^3k \tag{62}$$

$$= \frac{1}{\pi^2\hbar^3} \int_0^{k_F} \sqrt{m_e^2c^4 + k^2c^2} k^2 \mathrm{d}^3k \tag{63}$$

This integral can be solved by repeated partial integration. The details are in the appendix A.2.

$$\epsilon_{elec}(k_F) = \frac{\epsilon_0}{8} \left[(2x^3 + x)(1 + x^2)^{1/2} - \sinh^{-1}(x) \right] \tag{64}$$

with $x := \frac{k_F}{m_e c}$ and $\epsilon_0 := \frac{m_e^4 c^5}{\pi^2\hbar^3}$.
The next step is to get an equation for the pressure as a function of k_F. The calculations

for this can also be found in the appendix and I will just write down the solution here.

$$p(k_F) = \frac{\epsilon_0}{24}\left[(2x^3 - 3x)(1+x^2)^{1/2} + 3\sinh^{-1}(x)\right] \tag{65}$$

With the definition of x eq. 65 can be approximated in the leading order term x^4 to (see [34] for more details)

$$= \frac{\epsilon_0}{12}x^4 = \frac{\epsilon_0}{12}\left(\frac{k_F}{m_e c}\right)^4 \tag{66}$$

With the definition of k_F, ϵ_0 and the assumption that the mass density is dominated by the nucleons (i.e. $\frac{\rho_{star}}{c^2} \approx \epsilon$), one gets

$$p_{\text{rel}}(\epsilon) = K_{\text{rel}}\epsilon^{4/3} \tag{67}$$

$$K_{rel} = \frac{\hbar c}{12\pi^2}\left(\frac{3\pi^2 Z}{m_N c^2 A}\right)^{4/3} \tag{68}$$

Eq. 67 is called a relativistic EoS. With a high kinetic energy of the electrons, the central pressure becomes large and the star can support a higher mass before getting unstable.

In the second, non-relativistic case (where $k_F \ll m_e$) one can Taylor expand around small x. Orders of x^3 cancel and x^5 is the lowest order.

$$K_{nonrel}\epsilon^{5/3} = p_{nonrel}(\epsilon) = \frac{\epsilon_0}{24}\frac{8}{5}x^5 \tag{69}$$

$$\Rightarrow K_{nonrel} = \frac{\hbar^2}{15\pi^2 m_e}\left(\frac{3\pi^2 Z}{m_N c^2 A}\right)^{5/3} \tag{70}$$

This non-relativistic EoS leads to white dwarfs with lower masses as the central pressure becomes smaller. The maximum radius of the stars will become larger as one can see in fig. 2.
It is important to note that both relativistic and non relativistic degenerate pressure have no temperature dependency. This is because one assumes a completely degenerate electron gas where the occupation probability is independent of its temperature. In reality the temperature does not remain zero, so that decoupling of the mechanical structure of the star (which is determined by the Fermi distribution) and its thermal properties are not perfect (because of $E_F \gg k_B T$) [4].

3.2 COMPARISON OF RELATIVISTIC AND NON-RELATIVISTIC EOS

In the following section I will discuss different EoS and their impact on the behaviour of the maximum mass and radius of a white dwarf. I will use the two different EoS for a free electron gas that were derived in the previous section. We will see that the maximum mass of a white dwarf in the relativistic case does not depend on the starting pressure at $r = 0$ but remains a constant value, known as the Chandrasekhar mass. In the non relativistic case the maximum mass increases with a higher interior pressure.

3.2.1 *Non relativistic EoS*

The relation of the mass and the degenerate electron pressure is called mass-volume relation. An approximate relationship can be obtained by assuming that the density ρ is a constant and equating the degenerate electron pressure $p_{\text{nonrel}}(R)$ (eq. 69) can be equated with the central pressure P_c in the interior of the star:

$$P_c(R) = p_{\text{nonrel}}(R) \tag{71}$$

With eq. 91, P_c can be derived[1]:

$$\begin{aligned} \int_{P_c}^{0} \mathrm{d}p &= -\int_{0}^{M} \frac{Gm}{4\pi r^4}\,\mathrm{d}m \\ \Leftrightarrow \quad P_c(r) &= \frac{GM}{4\pi r^4} \\ \Rightarrow \quad \frac{\mathrm{d}P_c}{\mathrm{d}r} &= -\frac{GM}{4\pi r^2 r^3} \end{aligned}$$

differentiating P_c with respect to r, using the relation $M = \rho 4\pi r^2$ and integrating again for r yields

$$\begin{aligned} \Rightarrow \quad P_c(R) &= -\int_{0}^{R} \frac{GM\rho}{r^2}\mathrm{d}r = -\frac{4}{3}\pi G\rho^2 r \\ \Leftrightarrow \quad P_c(R) &= \frac{2}{3}\pi G\rho^2 R^2 \end{aligned}$$

Now equating both expression (eq. 71) and applying some simple algebraic transformations yields

$$R^2\rho^{\frac{1}{3}} = \text{const.} \quad \Leftrightarrow \quad R^3 M = \text{const.} \tag{72}$$

This is called mass-volume-relation and is a result of the star deriving its support from electron degeneracy pressure which is required to support a more massive star [4].
In fig. 2, three different central pressures have been considered and used as starting parameters to solve the the TOV-equation. Larger central density lead to a smaller maximum radius and a higher maximum mass. This confirms relation 72 where a constant density had been assumed (even though this is not strictly the case here).
Different pressures in the stellar interior lead to different results. The vertical lines represent the maximum mass (right axis) and the curved line (left axis) indicates the decrease of pressure while moving away from the stellar interior. The EoS of a free degenerate electron gas for non relativistic white dwarfs has been used (eq. 69).

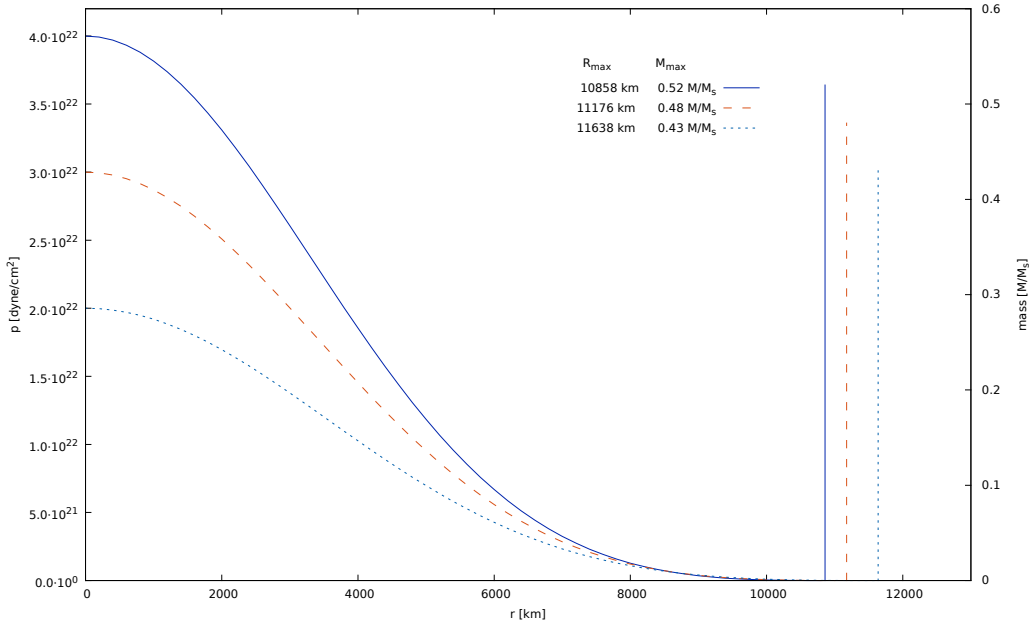

Figure 2: Masses and radii for three different starting pressures with a non relativistic EoS

[1] R is the radius outside the star and M the corresponding mass outside of the star. One uses the boundary conditions $P(R) = 0$, $M(0) = 0$ and $R_c = 0$

3.2.2 *Relativistic EoS and Chandrasekhar mass*

From here it is easy to derive the Chandrasekhar mass. Again one equates the degenerate electron pressure with the estimate of the central pressure P_c. This time one uses the relativistic polytrope (eq. 67) where $k_F \gg m_e$ and obtains

$$\frac{\hbar c}{12\pi^2}\left(\frac{3\pi^2 Z}{m_N c^2 A}\right)^{4/3} \cdot \left(\frac{\rho}{c^2}\right)^{4/3} = \frac{2}{3}\pi G\rho^2 R^2$$

Sorting by constants leads to an radius-independent mass M of the star, which is quiet remarking (ρ has been substituted with $\rho = M/4\pi r^2$). This is called the Chandrasekhar limit

$$M_{\mathrm{Ch}} = 1.44 M_S \tag{73}$$

As in the previous plot, maximum mass and radius have been plotted with increasing the inner pressure P_c, this time with more values. The mass of degenerate relativistic matter stays constant and its value confirms the value of the Chandrasekhar mass.

For fig. 3 an EoS for electron degenerate relativistic matter has been used as derived earlier. On the right side, the Chandrasekhar mass is marked. The x-axis has been plotted on a log scale. The interior pressure of the star is now higher than in the previous plot as the kinetic energy of the electrons is much higher then their rest mass.

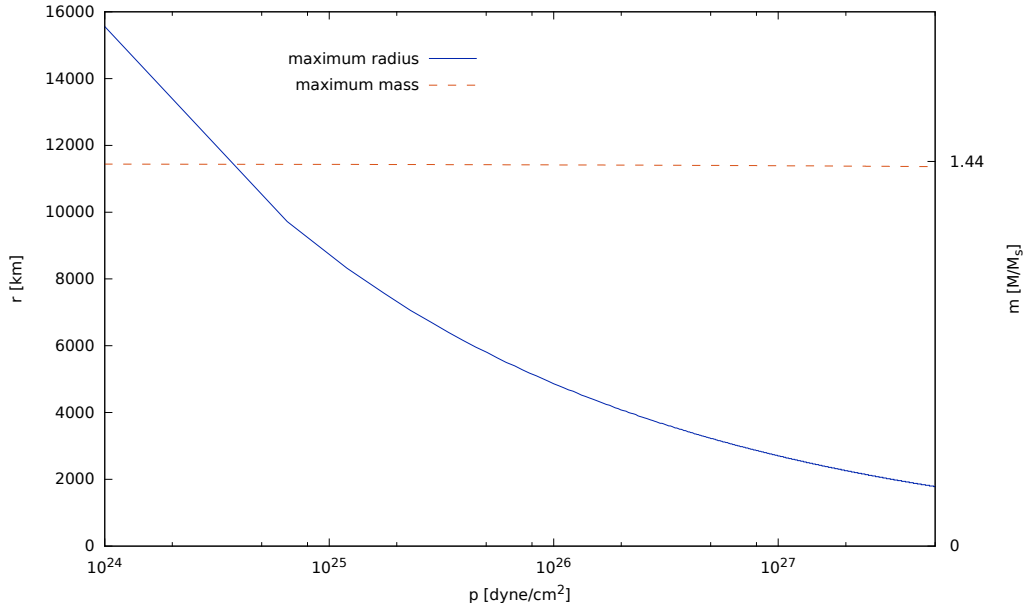

Figure 3: Mass-radius relation of a relativistic EoS in dependence of the starting pressure

For the sake of completeness, the non relativistic polytrope is also plotted (fig. 4) with the same axis labels as in fig. 3. Here, the masses increase with increasing pressure while the radius is decreasing (same properties as in fig. 2). One can also see that the size of these stars is much bigger than the size of relativistic stars

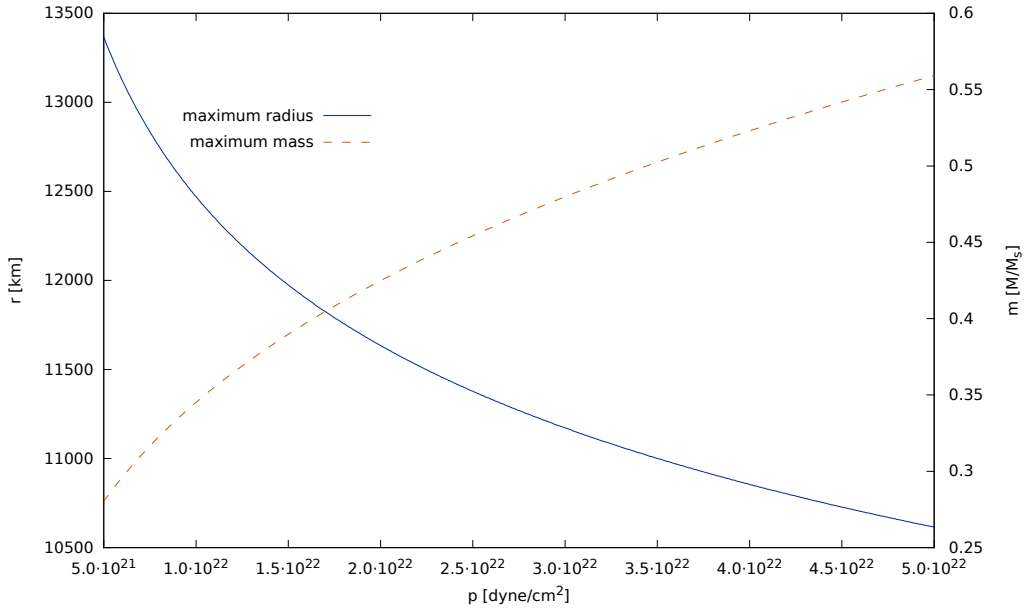

Figure 4: Mass-radius relation for a non relativistic EoS in dependence of the starting pressure

3.2.3 *Pure neutron stars*

For neutron stars, one can calculate an EoS by looking at a Fermi gas of degenerate neutrons. The calculation for $p(\epsilon)$ is similar to the one for white dwarfs and can be found here [15]. The following plot (5) is for a non relativistic gas. The initial staring pressures are much higher than the ones for white dwarfs.

$$K_{\text{nonrel}} = \frac{\hbar^2}{15\pi^2 m_n}\left(\frac{3\pi^2}{m_n c^2}\right)^{5/3}$$

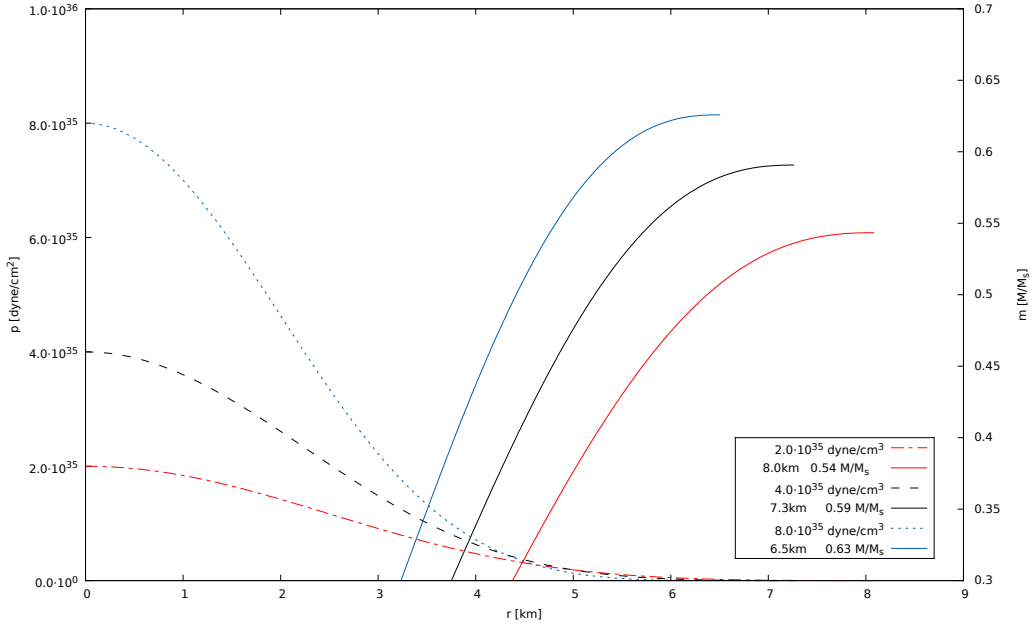

Figure 5: Masses and radii for a pure neutron star

4

SKYRME PARAMETRIZATION

The Skyrme parametrization is a mean field approach hence provides a consistent and physically sensible method to study interacting systems where correlations are less important [22]. It can be derived out of the Hartree-Fock equations. "The key to the basic Hartree-Fock method is the assumptions it makes about the form of the electron wave function. It will be assumed that there are a total of I electrons in orbit around a number of nuclei" [38]. In this case, the nucleon-nucleon interaction potential is described by the Skyrme parametrization that has the following form

$$V(x,y) = \delta^3(x-y)\left(\frac{1}{6}t_3 n - t_0\right)$$

One can split the single particle energy densities for a Number N_p of protons and N_n neutrons into

$$\epsilon_k^{(p)} = \frac{k_p^2}{2m_p} + \left(\frac{1}{6}t_3 n - t_0\right)\frac{1}{V}\left(\frac{N_p}{2} + N_n\right)$$

and

$$\epsilon_k^{(n)} = \frac{k_n^2}{2m_n} + \left(\frac{1}{6}t_3 n - t_0\right)\frac{1}{V}\left(\frac{N_n}{2} + N_p\right),$$

One assumes that all levels up to the Fermi momentum k_F are occupied (k_p and k_n respectively stand for the Fermi edge of protons and neutrons).
n describes the total number density of the systems $n = (N_p + N_n)/V$, t_0 the attractive two particle nuclear interaction and $t_3 n$ describes the repulsive many-body interaction. t_3 and t_0 are empirical constants which are adjusted to the experimental binding energies and radii [3].
There are several sets of parameters for t_0 and t_3, resulting from different fits [32]. The following values will be used in the later calculations: $t_0 = 1024.1$ MeVfm^3, $t_3 = 14600.8$ MeVfm^6, as was obtained here [34].
Detailed explanations of the Skyrme parametrization are found for example here [3], [39].
The energy density under the assumption of pure neutron matter, has the following form [34]

$$\epsilon(n) = m_n n + \frac{3}{10m_n}(3\pi^2\hbar^2)^{2/3}n^{5/3} + \frac{t_3}{24}n^3 - \frac{t_0}{4}n^2$$

and with the thermodynamical relation

$$p(n) = n\frac{\mathrm{d}}{\mathrm{d}n}\epsilon(n) - \epsilon(n),$$

one gets

$$p(n) = \frac{2}{10m_n}(3\pi^2\hbar^3)^{2/3}n^{5/3} + \frac{t_3}{12}n^3 - \frac{t_0}{4}n^2$$

In the following plot one can see the EoS of the Skyrme parametrization and the EoS of a free neutron gas. Also plotted is the fraction of the number density n with the nuclear saturation density n_0. This is the density at which nuclear matter is bound at zero pressure [6].
One can see that at low densities, the Skyrme EoS has a higher energy density than the EoS for a free neutron gas, whereas at higher densities it has lower values for the energy density.

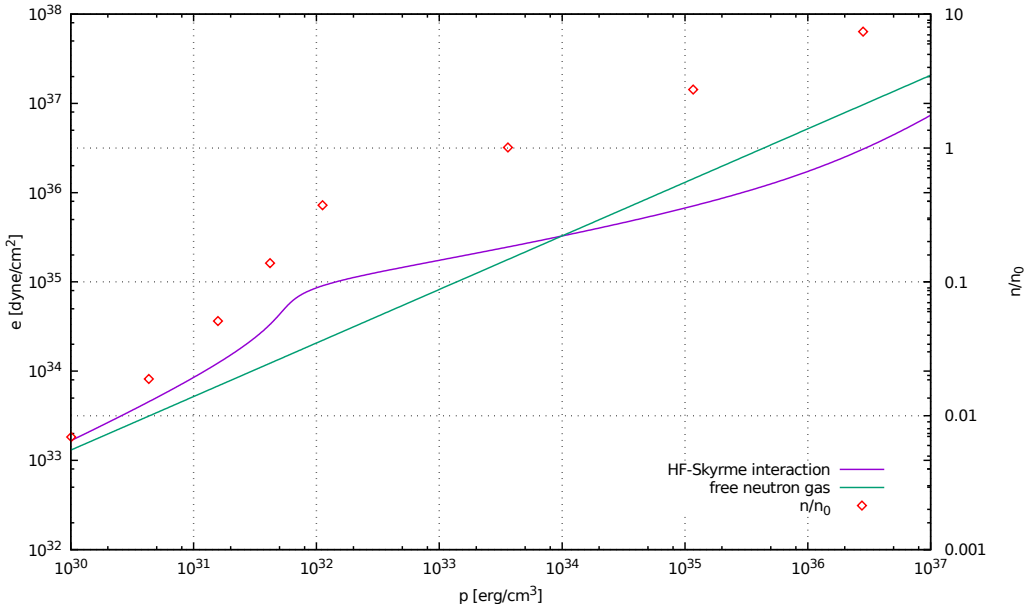

Figure 6: Skyrme parametrized EoS

In the following plot one can see the maximum masses of a star and its corresponding radius. The maximum mass is slightly under two sun masses with a radius at around 11 *km*.

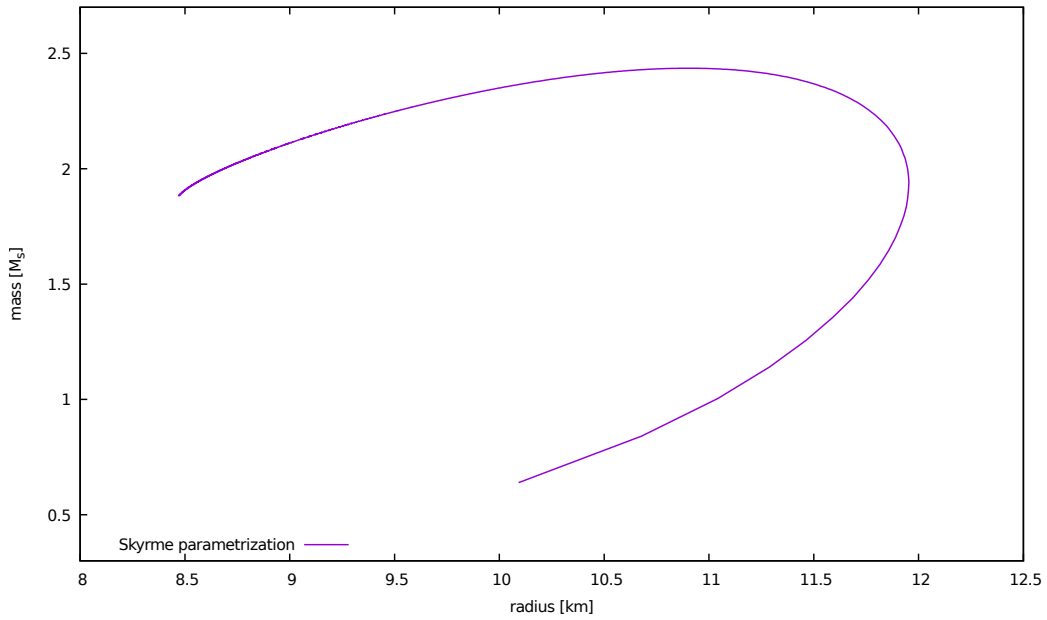

Figure 7: Mass radius relation

5

INTRODUCTION TO GROUP AND FIELD THEORY

5.1 MULTIPLETS

The quantum states of elementary particles conserve symmetries under specific transformations. One summarises these transformations into symmetry groups whose linear operators $D(g)$ do not lead the states $|\Psi\rangle$ out of their original space U [33]

$$\forall\, |\Psi\rangle \in U\,, \forall g \in G: \quad D(g)\,|\Psi\rangle \in U,$$

whereby U is a subspace of the Hilbert space $\mathcal{H}$ and $D(g)$ is a representation of an element g of G. U is then called an invariant subspace in relation to the symmetry group G. One important attribute of groups is their irreducible representations. An irreducible subspace $\mathcal{M} \subset \mathcal{H}$ contains no further invariant subspaces despite itself. The linear operators of the group elements $g \in G$ which act on the elements of M are then called irreducible representation [21].
The term multiplet which will appear later, is an irreducible subspace [13]. A Casimir operator is closely related to a multiplet. It is an operator $\hat{C}$ which commutes with all group elements $g \in G$

$$[\hat{C}, g] = 0$$

For example the square of the angular momentum $\vec{\hat{L}}^2$ is a Casimir operator. Its eigenvectors span the multiplets of the group $SU(2)$ (the representations of the group elements of $SU(2)$ are $\hat{U}_R(\vec{\Phi}) \exp\left(-\frac{i}{\hbar}\vec{\Phi}\vec{\hat{L}}\right)$) and its eigenvalues are

$$\hat{\vec{L}}^2\,|l\rangle = \hbar^2 l(l+1)\,|l\rangle$$

For a given quantum number of the angular momentum there exist several degenerate states which form the multiplets. The states of the multiplets are determined through the quantum number m (and a fixed l). m can have the values $-j, -j+1, ...j-1, j$ which makes a total of $(2l+1)$ eigenstates for $\hat{\vec{J}}^2$. Therefore the number of states of the multiplet are

$$\begin{aligned} l = 0 &\rightarrow \text{singlet} \\ l = \frac{1}{2} &\rightarrow \text{doublet} \\ l = 1 &\rightarrow \text{triplet} \\ &... \end{aligned}$$

There are gradual operators which transpose one state of one multiplet into another state one of the same multiplet [37]

$$\hat{J}_\pm\,|j\ m\rangle \sim |j\ m\pm 1\rangle$$

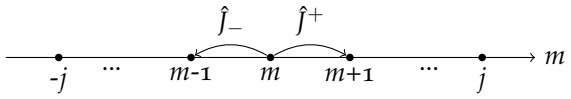

Figure 8: The quantum number m can be raised or lowered by $J_\pm$

For $SU(2)$ multiplets, there is the quantum number m which can be raised and lowered and quantifies a state. For $SU(3)$-multiplets, there are two quantum numbers (instead two dimensions there are now three so one can go up and down as well), namely T_3 and Y. The operators $\hat{Y}$ and $\hat{T}_\pm$ commute $\left[\hat{Y}, \hat{T_\pm}\right] = 0$ so that they have a common basis and the states of the multiplet can be characterized with the eigenvalues of the two operators $|T_3 Y\rangle$. In summary the following operators change between states within a multiplet with the following eigenvalues (more details here [33])

- $\hat{T}_\pm$ raises/lowers T_3 by $\hbar$, leaves Y unchanged
- $\hat{V}_\pm$ raises/lowers T_3 by $\pm\hbar/2$ and Y by $\pm\hbar$
- $\hat{U}_\pm$ lowers/raises T_3 by $\mp\hbar/2$ and raises/lowers Y by $\pm\hbar$

These operations can be shown as a diagram

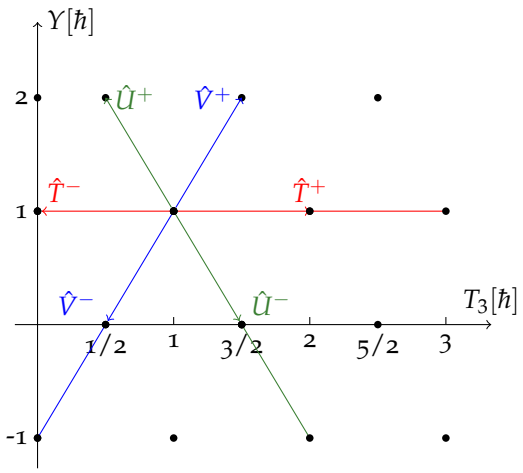

Figure 9: There are three lines. The red T-line on which $\hat{T}_\pm$ can raise or lower T_3 by $\pm\hbar$; The blue V-line where the values of T_3 can be raised or lowered by the operator $\hat{V}$ by $\pm\hbar/2$ while also Y gets changed by $\pm\hbar$; The green line, where $\hat{U}$ changes T_3 by $\mp\hbar$ and Y by $\pm\hbar$.

The shape of a multiplet in $SU(3)$ has the following properties [33, 35]

- 120 degrees symmetry
- edge of multiplet is convex

5.2 THE QUARK MODEL

There are six different flavors: up, down and strange and their anti-flavors ($\overline{u}$,$\overline{d}$,$\overline{s}$). One can show that if one assumes equal quark masses, the Lagrangian density (which contains now mass terms of the quarks) stays invariant under $SU(N_f)$-vector transformations. N_f is the number of flavours. This is called $SU(N_f)$-flavour-symmetry. In reality the masses of the u and d quark are nearly identical. However the s quark is much heavier. On an energy scale of hadrons of ~ 1 GeV this difference is still vanishing small. Therefore one can roughly assume a $SU(3)$-flavor-symmetry [28, 33]. All other quarks are at an energy

scale larger $m_h \sim 1\ GeV$ so that there is no good approximation for a symmetry higher than $SU(3)$. Overview of the quark masses [33]:

$$\begin{aligned} m_u &\sim 2.5 \text{ MeV} \\ m_d &\sim 5 \text{ MeV} \\ m_s &\sim 105 \text{ MeV} \\ m_c &\sim 1.266 \text{ GeV} \\ m_t &\sim 4.198 \text{ GeV} \\ m_b &\sim 173.1 \text{ GeV} \end{aligned} \tag{74}$$

The $SU(2)$-flavour-symmetry, also called isospin-symmetry, assumes equal masses of u and d-quarks. In neutron stars this symmetry is broken due to a significant higher number of neutrons compared to protons. This affects the masses of neutron stars because the Fermi energy of the system is then higher due to the Pauli-blocking so that more pressure holds against the gravitational one. The star can therefore generate higher masses [8]. The quark model contains two types of hadrons. The baryons, which compose of three quarks and the mesons which compose of a quark-anti-quark pair $q\bar{q}$. Both hadrons are the eigenstates of the Hamiltonian $\hat{H}$ of the strong force [35]. In fig. 10, the quantum numbers T_3 and Y have been introduced for the $SU(3)_{\text{fl}}$-group[1]. Physically, $T_3 \equiv I_Z$ is the third component of the isospin-component and with the Gell-Mann-Nishijima-relation, Y can be identified as the hyper charge $Y = 2Q - I_Z$ (Q is the electric charge in terms of the elementary charge e) [25]. For construction of the multiplets of $SU(3)$ for the quark model, one assumes a $SU(3)$-flavour-symmetry thus one neglects the mass differences between u, d and s-quark [35].
The addition of single angular momenta is the product of states of different sub spaces $|j_1 j_2; m_1, m_2\rangle \equiv |j_1 m_1\rangle\,|j_2 m_2\rangle$. There are restrictions for the values of total angular momentum j [33]:

$$|j_1 - j_2| \leq j \leq j_1 + j_2. \tag{75}$$

For example two particles with angular momenta $j_1 = \frac{1}{2}$ and $j_2 = \frac{1}{2}$ form two doublets and together they couple to a total angular momentum, a singlet and a triplet [33] (because of equation 75, it follows that $j_{min} = 0$ and $j_{max} = 1$)

$$[2] \otimes [2] = [1] \oplus [3] \tag{76}$$

The decomposition of two (or more) angular momenta into higher multiplets of total angular momenta is called "Ausreduzierung" [33]. The singlet is the trivial presentation of $SU(2)$ thus no higher multiplets can be generated from it. The triplet is the smallest non trivial representation of $SU(2)$.
For the $SU(3)$-flavour-symmetry, the quark and anti quark triplet has the following form in the $Y - T_3$-plane:

[1] The subscript stands for flavor. There are also other SU(3) symmetries like the colour symmetry where an additional colour is assigned to each quark flavor

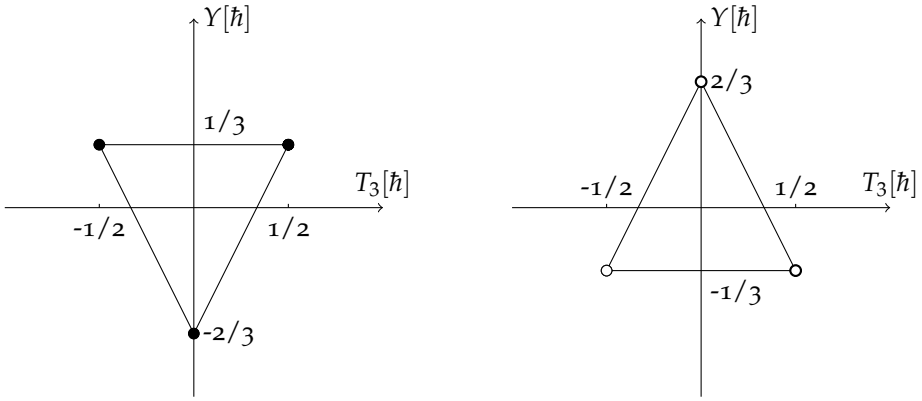

Figure 10: The quark triplet (left) and the anti quark triplet (right). Each dot (left side: black, right side: white) is an eigenstate in the $Y - T_3$ plane, see eq. 77 - 82.

Each eigenstate $|T_3 Y\rangle$ corresponds to one flavor (up, down, strange) and can be transformed into a state with another flavor but not out of its multiplet.

$$|u\rangle \equiv |\frac{1}{2}\frac{1}{3}\rangle \tag{77}$$

$$|d\rangle \equiv |-\frac{1}{2}\ \frac{1}{3}\rangle \tag{78}$$

$$|s\rangle \equiv |0 - \frac{2}{3}\rangle \tag{79}$$

The anti-quarks have with their 'anti-flavor'

$$|\overline{u}\rangle \equiv |-\frac{1}{2} - \frac{1}{3}\rangle \tag{80}$$

$$|\overline{d}\rangle \equiv |\frac{1}{2} - \frac{1}{3}\rangle \tag{81}$$

$$|\overline{s}\rangle \equiv |0\ \frac{2}{3}\rangle \tag{82}$$

5.2.1 *Baryons*

Baryons are composed of three quarks so that the product of the three triplets need to be 'ausreduziert'

$$[3] \otimes [3] \otimes [3]$$

There are descriptive rules how to proceed graphically with the 'Ausreduzierung' of the multiplets. At each occupied point in the $T_3 - Y$-plane the other multiplet is set so that its centre is at one occupied place. For baryons one evaluates first the product $[3] \otimes [3]$:

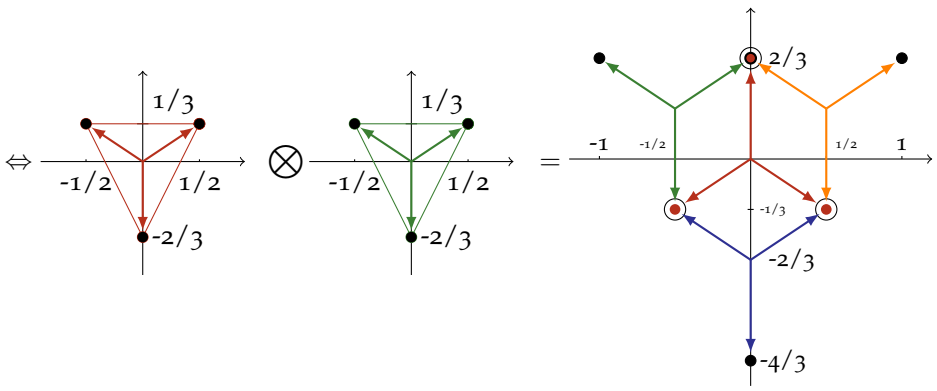

This graph composes a sextet and anti-triplet so that one can write $[3] \otimes [3] = [6] \oplus [\bar{3}]$

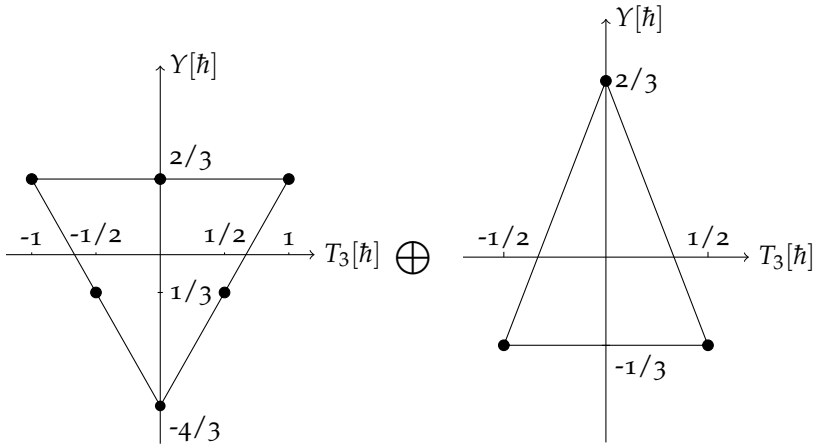

One can now evaluate $[3] \otimes [3] \otimes [3] = [3] \otimes \left[[6] \oplus [\bar{3}]\right]$ with the same rules to $[1] \oplus [8] \oplus [8] \oplus [10]$ (the explicit derivation can be found here [33]). Baryons can occur as singlets, octets or decuplets [35].

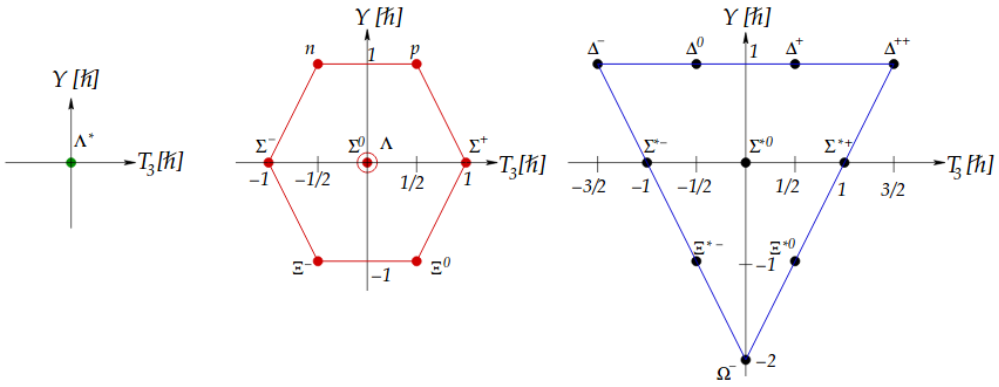

Figure 11: baryon singlet, octet and decouplet (from left to right)[2]

[2] [33]

5.2.2 *Mesons*

Mesons compose of a quark -anti-quark pair $q\bar{q}$

$$[3] \otimes [\bar{3}] = [1] \oplus [8]$$

Again, one 'ausreduziert' the two triplets and obtains a singlet and an octet.

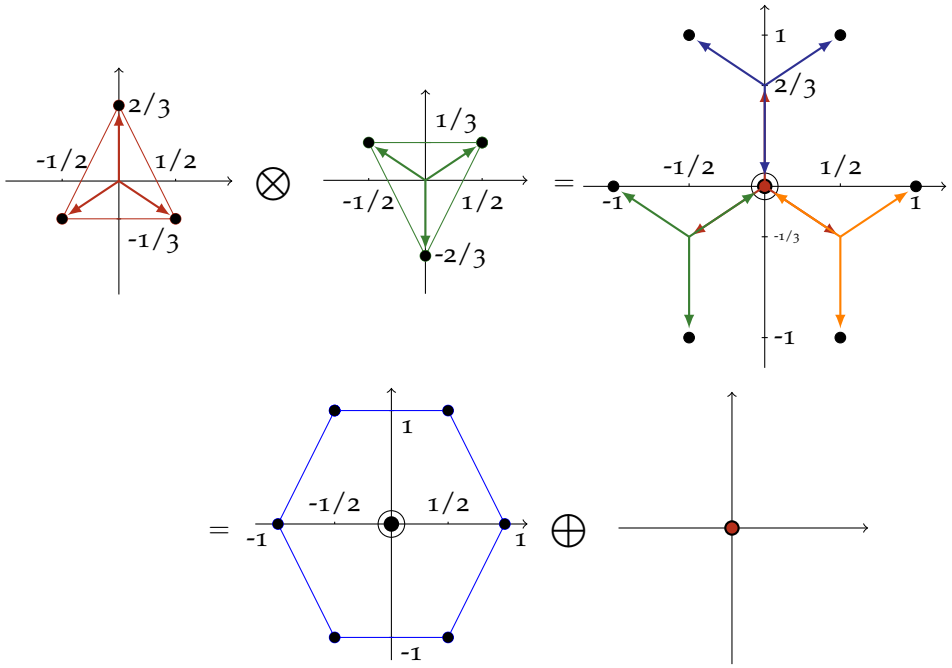

One distinguishes between scalar mesons, pseudo scalar mesons, vector mesons and axial-vector mesons. They all have the same flavor quantum number but a different total angular moment. Their classification J^{PC} is made by isospin I, spin J, parity P and charge C [33]:

- scalar mesons $J^{PC} = 0^{++}$
- pseudo-scalar mesons $J^{PC} = 0^{+-}$
- vector mesons $J^{PC} = 1^{--}$
- axial-vector-mesons $J^{PC} = 1^{++}$

5.3 LAGRANGIAN FORMULATION OF FIELDS

The key principle of the theory of fields is the minimum of action

$$\delta S = 0,$$

δS is the variation of the action. The action is defined as the integral over the Lagrange density

$$S = \int \mathcal{L}[\Phi(x), \partial_\mu \Phi(x)] \mathrm{d}^4 x$$

With the variation of the action inside the integral, one can derive the Euler-Lagrange equation which reads [36]

$$\frac{\partial \mathcal{L}}{\partial \Phi(x)} - \partial_\mu \frac{\partial \mathcal{L}}{\partial(\partial_\mu \Phi)} = 0 \tag{83}$$

If one has the Lagrangian (density) of a theory, one can apply the Euler-Lagrange equation to it and obtain different field equations. In the following I will introduce some

Euler-Lagrange equations for non-interacting fields which are also used in the non linear sigma model[3].

5.3.1 *Klein-Gordon Equation*

The Lagrangian density for an uncharged, free field $\sigma(x)$ reads

$$\mathcal{L}_\sigma = \frac{1}{2}(\partial_\mu \sigma(x)\partial^\mu \sigma(x) - m_\sigma^2 \sigma^2(x)) = 0$$

Inserting $\mathcal{L}_\sigma$ into the Euler-Lagrange equation (equation 83) yields the Klein-Gordon-equation

$$(\Box + m_\sigma^2)\sigma(x) = 0$$

It describes Spin-0 particles (like the Boson).

5.3.2 *Procca Equation*

For vector fields ω_μ with a mass m_μ one defines kind of a strength tensor which contains the derivatives $\omega_{\mu\nu}$ of the field [36]

$$w_{\mu\nu} = \partial_\mu \omega_\nu - \partial_\nu \omega_\mu.$$

The full Lagrangian reads

$$\mathcal{L}_\omega = -\frac{1}{4}\omega_{\mu\nu}\omega^{\mu\nu} + \frac{1}{2}m_\omega^2 \omega_\mu \omega^\mu.$$

Inserting into the Euler-Lagrange equation and multiplying with ∂^μ yields the so called Proca Equation

$$(\Box + m_\mu^2) = 0 \tag{84}$$

It describes particles with spin 1 (like the photon).

5.3.3 *Dirac equation*

All fermions can be described with the Dirac Lagrangian

$$\mathcal{L} = \overline{\Psi}(i\gamma^\mu \partial_\mu - m_f)\Psi = 0,$$

where m_f is the mass of the fermion. The Euler-Lagrange equation reads [36]

$$(i\gamma^\mu \partial_\mu - m_f) = 0$$

5.4 STAR MATTER

The matter inside a neutron star has the following properties

- charge neutrality: This is necessary for the star to be stable. The total charge of the star should lie below a certain limit where the coulomb repulsive force is bigger than the gravitational attractive force at the surface of the star. [4]

[3] Because nuclear matter is a strong interacting medium, there are much more terms necessary which also take interactions into counter.

[4] But because of high densities and pressure, strong electrical fields can occur. To read more about neutron stars and the effects of electric charge on a polytropic equation of state, see here [23]

- baryonic number conservation: The number of baryons of all incoming particles is the same as the sum over baryons of all particles resulting from the reaction [27]
- β equilibrium: The β decay transforms neutrons into protons and vice versa under emittance of an electron or positron and neutrino. The equilibrium condition in neutron stars makes it possible to write single chemical equilibrium equations for the different particles as a function of a small number of chemical potentials depending on each other [8].
- chemical equilibrium: The number of particles of each kind is not conserved, but they are created and annihilated through specific reactions happening at the same rate in both directions

Also an important property of star matter (specifically neutron stars) is that the strangeness quantum number is not constrained and determined by the condition of β equilibrium [16].

5.5 NON-LINEAR SIGMA MODEL

The non-linear-sigma-model is an effective relativistic quantum model, that describes a system of hadrons interacting via σ scalar and ω_μ vector mesons. To solve the equations which arise from this model, one uses a mean field approximation where the meson field is replaced by the mean value of its ground state $\langle\sigma\rangle$ and $\langle\omega_\mu\rangle$ [36]. The Lagrangian is composed of

$$\mathcal{L} = \mathcal{L}_{kin} + \mathcal{L}_{int} + \mathcal{L}_{scal} + \mathcal{L}_{vec} + \mathcal{L}_{SB} - U \tag{85}$$

In the following I give a brief overview over the single terms in the Lagrangian. I will not go in any detail, an explicit explanation of the single terms can be found here [8].

The first term $\mathcal{L}_{kin}$ is the kinetic energy term which contains

- Dirac kinetic term for baryon octet
- Klein-Gordon kinetic term for scalar meson multiplet
- interaction term between scalar and pseudoscalar mesons (which also contains the kinetic term for the pseudoscalar meson octet)
- Klein-Gordon kinetic term for the pseudoscalar meson singlet
- Klein-Gordon kinetic term for the scalar-isoscalar glueball field
- Proca kinetic term for the vector meson multiplet
- Proca kinetic term for the axial vector meson multiplet

The second term $\mathcal{L}_{int}$ in the Lagrangian is the interaction term between baryons and mesons. It is divided into a

- interaction term $\mathcal{L}_{Bscal}$ between baryons and scalar mesons
- interaction term $\mathcal{L}_{Bvec}$ between baryons and vector mesons

The baryons, which are the degrees of freedom in this model, interact with each other via an exchange of scalar mesons (ρ, δ, ζ, $\mathcal{X}$) and vector mesons (ρ, ω, Φ) [9].
The third and fourth part of the Lagrangian are the self interaction terms

- self interaction term $\mathcal{L}_{scal}$ for spin-0 scalar and pseudo scalar mesons
- self interaction term $\mathcal{L}_{vec}$ for spin-1 vector and pseudo vector mesons

$\mathcal{L}_{SB}$ is a chiral symmetry breaking term. It arises from the "Goldstone modes", which appear due to a spontaneously broken continuous symmetry. The explicit symmetry breaking term eliminates these effects [8].

The last term U is the potential for the Polyakov loop [10]. The Polyakov-loop potential at zero temperature is defined as

$$U = a_1 \mu^4 \Phi^2.$$

It is an order parameter for deconfinement (i.e. its value shows whether or not symmetry broken)

$$\Phi = \begin{cases} 0 & \text{symmetry respected} \\ > 0 & \text{symmetry spontaneously broken} \end{cases} \tag{86}$$

The effective masses for baryons and quarks are effected by the presence of the Polyakov loop

$$m_b^* = g_{b\sigma} + g_{b\delta}\tau_3\delta + g_{b\zeta}\zeta + \delta m_b + g_{b\Phi}\Phi^2 \tag{87}$$

$$m_q^* = g_{q\sigma} + g_{q\delta}\tau_3\delta + g_{q\zeta}\zeta + \delta m_q + g_{q\Phi}(1-\Phi) \tag{88}$$

The $g_{b/q,i}$ are the quark couplings to the different fields. $\delta m_{u/d} = 5$ MeV and $\delta m_s = 150$ MeV are small explicit mass terms of the quarks. The Polyakov-loop has higher baryon masses for a non-vanishing Polyakov-field, the baryons are then suppressed at high densities [8]. Similarly if the quark-masses are smaller, they are more likely to exist in the high density regime.
In the following section the temperature is approximated to zero so that the Fermi energy is just given by the chemical potential. The Fermi energy is then the energy which is necessary to add or remove a to or from the system. If the chemical potential is very high because many particles are in a system (high density), a big amount of energy is necessary to add a new particle. It can then be more advantageous for the system (i.e. lower energy) to convert a particle into another one whose chemical potential is then lower. At low densities nucleons appear. Because star matter is mainly composed of neutrons and protons, those will dominate the regime on the hadronic phase. With increasing chemical potential, depending on the parameters, a phase transition to quark matter can occur where quarks are then deconfined. The symmetry is then spontaneously restored and the Polyakov loop has a non zero value.
The appearance of hyperons can also occur in the hadronic phase when the nucleon chemical potentials are higher than the mass difference between nucleons and hyperons (plus their lower chemical potential) [1]. This causes a softening of the EoS (a soft equation of state has a lower decrease in pressure for a constant change in density than a stiff one). As already mentioned above, converting to hyperons can be energetically favourable if the chemical potential of the nucleons is very high, so that the energy that would go into a kinetic and potential one (leading to a higher pressure), is instead "stored" in the mass difference of the two species [1].
Also interesting is the abundance of strange quarks. Their quantitative appearance is an important measure for the deconfined matter phase (a large number is an indicator that a phase transition to quark gluon plasma has occurred). They only appear in pairs of quarks-antiquarks ($s\bar{s}$) on the assumption that the hadronic collision time is too short for the weak interaction to convert from weak interaction conversion to strangeness [31].

6

RESULTS

In this chapter I will show several EoS for which I have tested different parameters a_1, $g_{q\omega}$ and effective masses that are shown in the tables below. One will see that if a phase transition exists, it appearance strongly depends on the different values for the coupling constants. This determines the maximum mass of a neutron star. The phase transition will mostly be of first order (jump in the energy density). Later on the parameter will be modified so the no phase transition occurs. If $\Delta\epsilon$ is very high, the star gets unstable due to an increase in gravitational pressure (while pressure is constant, regarding a first order phase transition). By decreasing the Polyakov loop, a second order phase transition will occur.
The plots (fig. 12-42) show the results for the particle occurrences and the corresponding EoS's of the different parameters as chosen in the tables 1-5. The graphs with different colored lines (see i.e. fig. 12) show the particles that occur in dependence of the chemical potential μ (on the x-axis). The y-axis displays the fraction of the single particle density divided by the density of the baryon density. The EoS is plotted (red dotted) i.e. in fig. 13) as well as the Polyakov loop (black lined).

6.1 VARYING a_1 OF THE POLYAKOV LOOP

In the following section I will show results for which a_1 was varied while all other constant were held constant. I chose five different values for a_1, ordered by size. In the table next to the coupling constant, I also display the gap in the energy density and the pressure where the phase transition occurs.

Table 1: Varying a_1

	g_σ^q	g_δ^q	g_ζ^q	g_ω^q	g_ρ^q	g_Φ^q	a_1	$\Delta\epsilon$[MeVfm^{-3}]	p_{pt}[MeVfm^{-3}]
t1.1	-3	0	-3	5.0	0	0	$2.34 \cdot 10^{-3}$	1493	291
t1.2	-3	0	-3	5.0	0	0	$3.12 \cdot 10^{-3}$	1097	160
t1.3	-3	0	-3	5.0	0	0	$3.28 \cdot 10^{-3}$	1021	142
t1.4	-3	0	-3	5.0	0	0	$3.51 \cdot 10^{-3}$	927	121
t1.5	-3	0	-3	5.0	0	0	$3.90 \cdot 10^{-3}$	1078	112

Before the phase transition, the star is mainly dominated by p and n and a smaller amount of Λ-baryons. After the phase transition, u and d quarks compose the star matter. There is a jump in the energy density at a corresponding pressure $p = 291$ MeV fm^{-3}. The gap is about 1493 MeV/fm^3. At the phase transition, the Polyakov-loop jumps from zero to a non-zero value, and quarks appear.

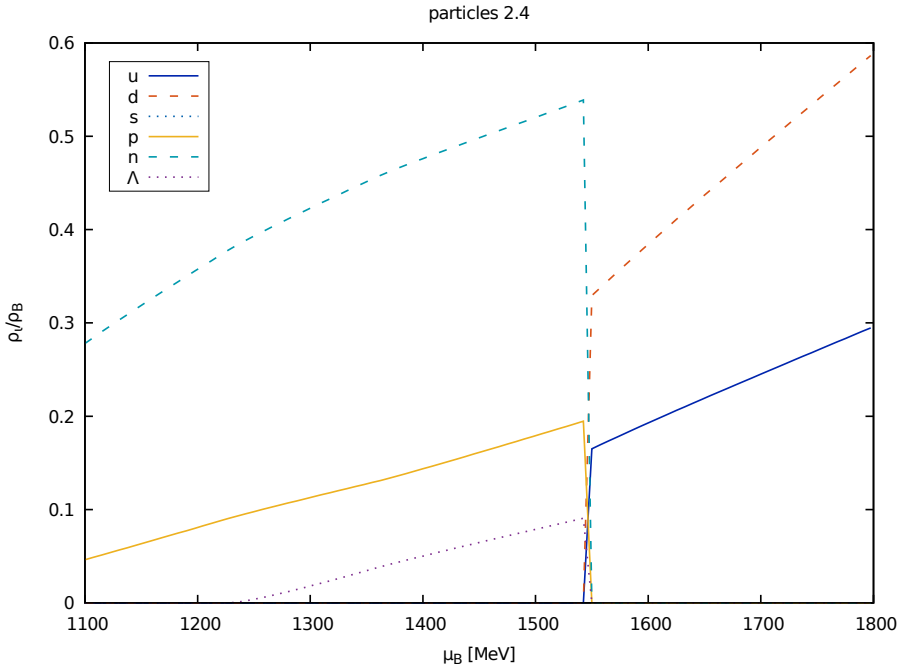

Figure 12: Particle densities (see t1.1 in table 1)

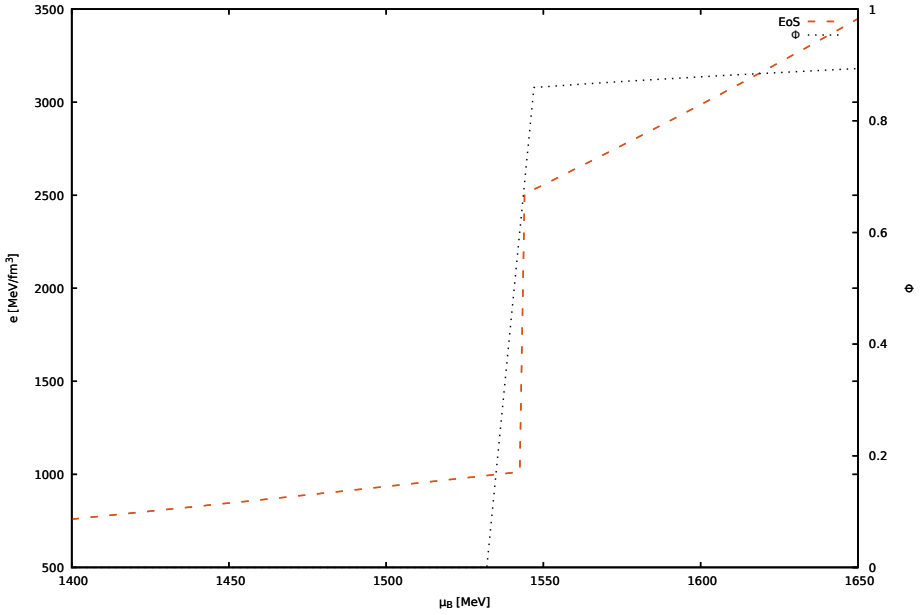

Figure 13: EoS and Polyakov loop (see t1.1 in table 1)

In fig. 14 and 15, the appearance of quarks is now at a slightly earlier chemical potential. Also notable is the smaller density of the p, n and Λ-baryons as well as the density of u and d quarks after the phase transition.

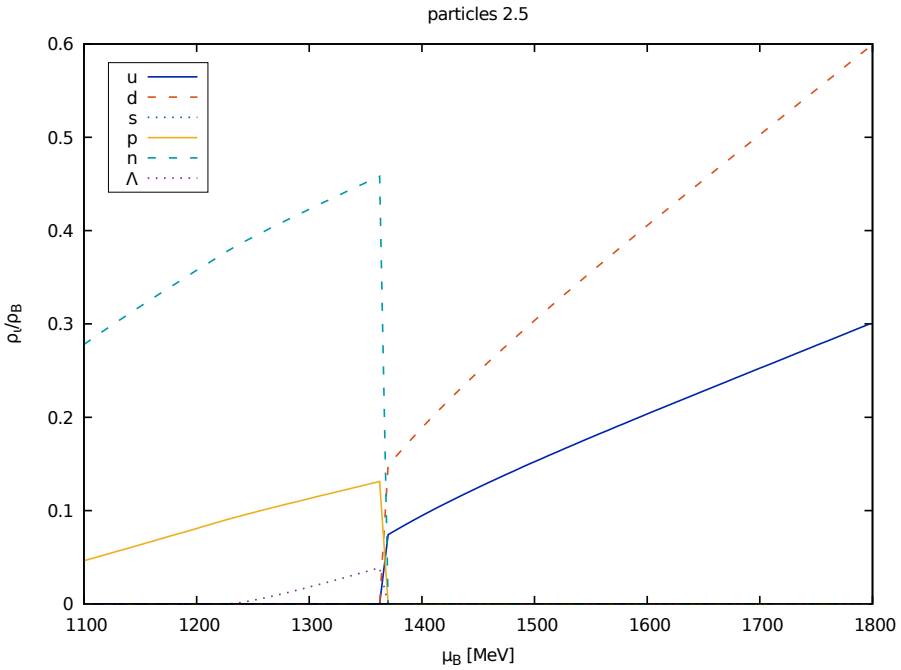

Figure 14: Particle densities (see t1.2 in table 1)

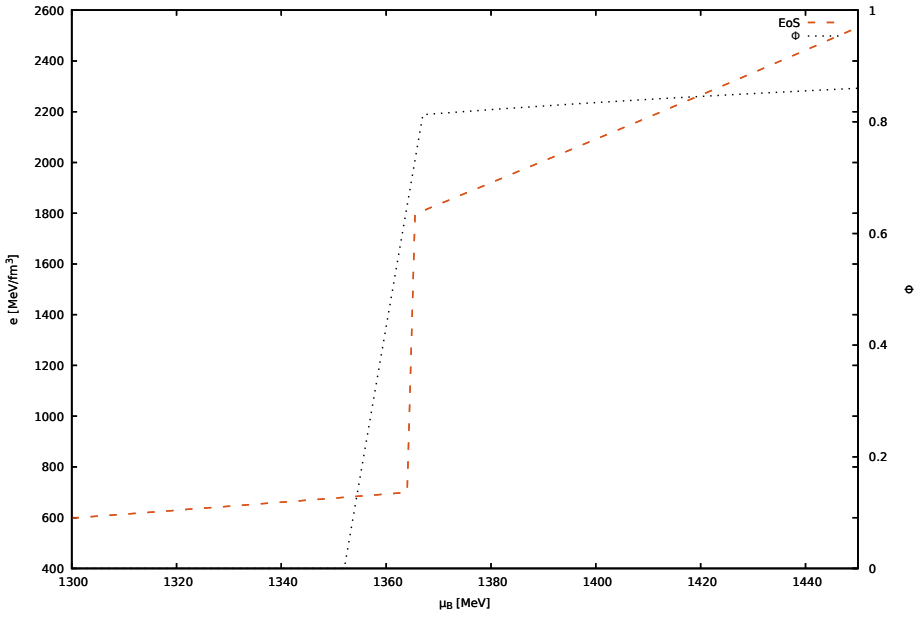

Figure 15: EoS and Polyakov loop (see t1.2 in table 1)

Fig. 16 and 17: The phase transition is again earlier and the jump in energy density is decreasing. There is no significant change in the particle densities.

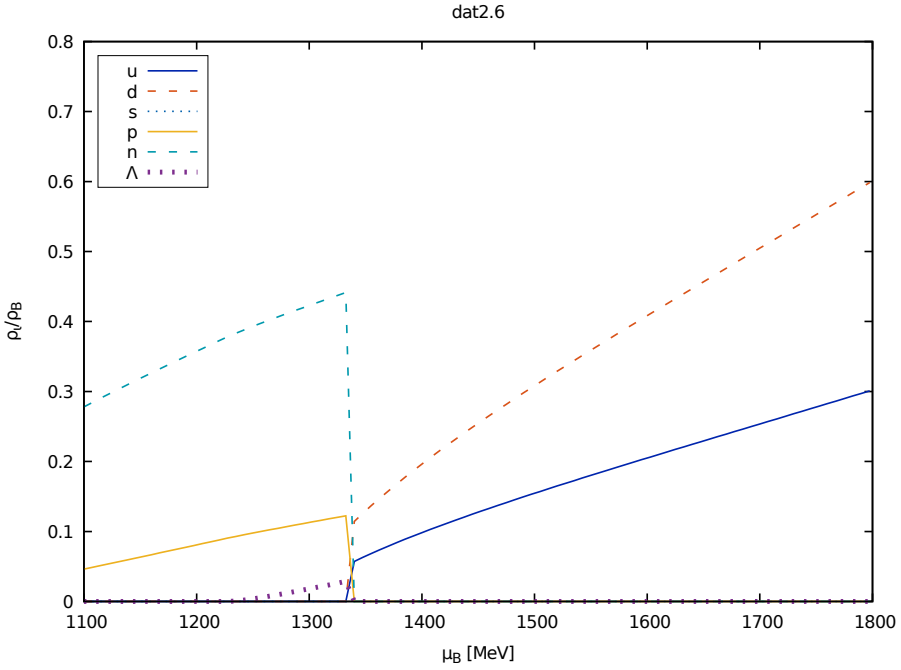

Figure 16: Particle densities (see t1.3 in table 1)

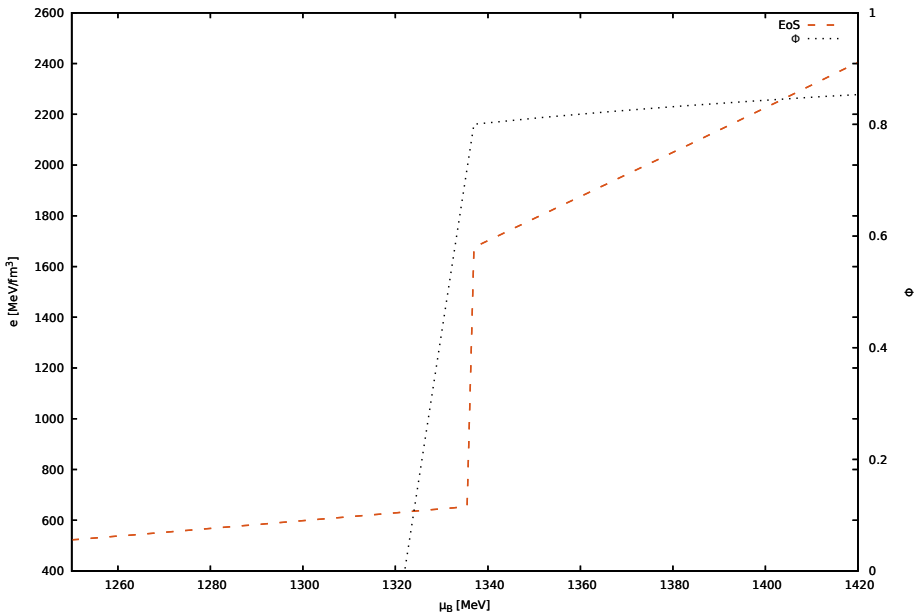

Figure 17: EoS and Polyakov loop (see t1.3 in table 1)

The phase transition in fig. 18 and 19 is further shifted to a lower chemical potential but there is no significant change in the single densities of the particles.

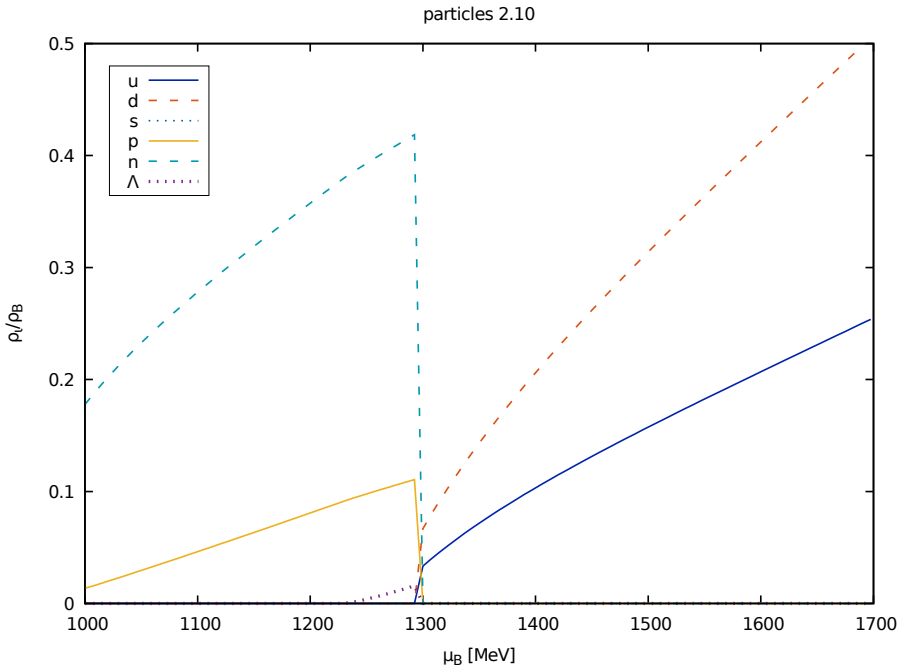

Figure 18: Particle densities (see t1.4 in table 1)

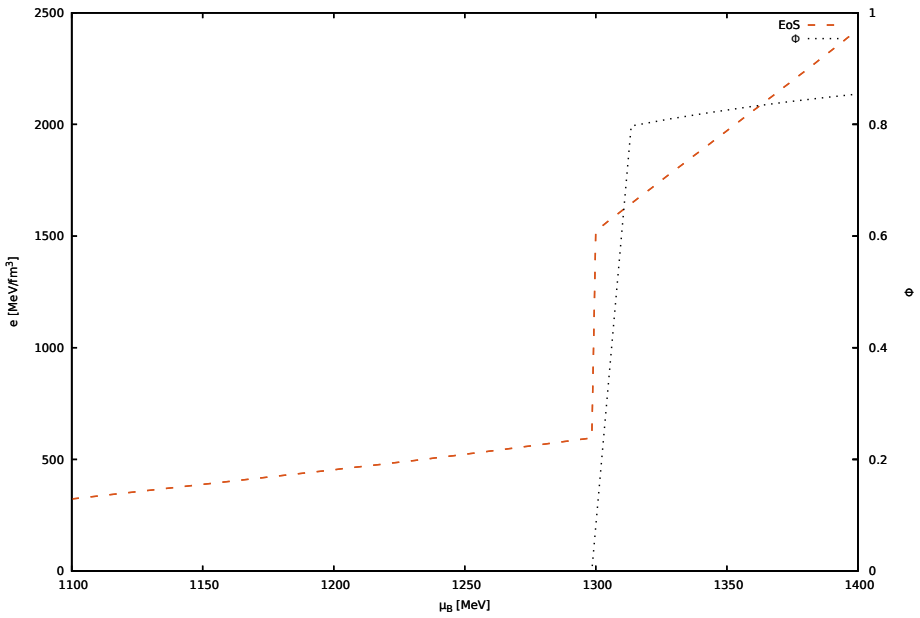

Figure 19: EoS and Polyakov loop (see t1.4 in table 1)

Fig. 20 and 21 show the same behavior as in the previous plots. The chemical potential at an earlier μ_B, no significant change in particle composition.

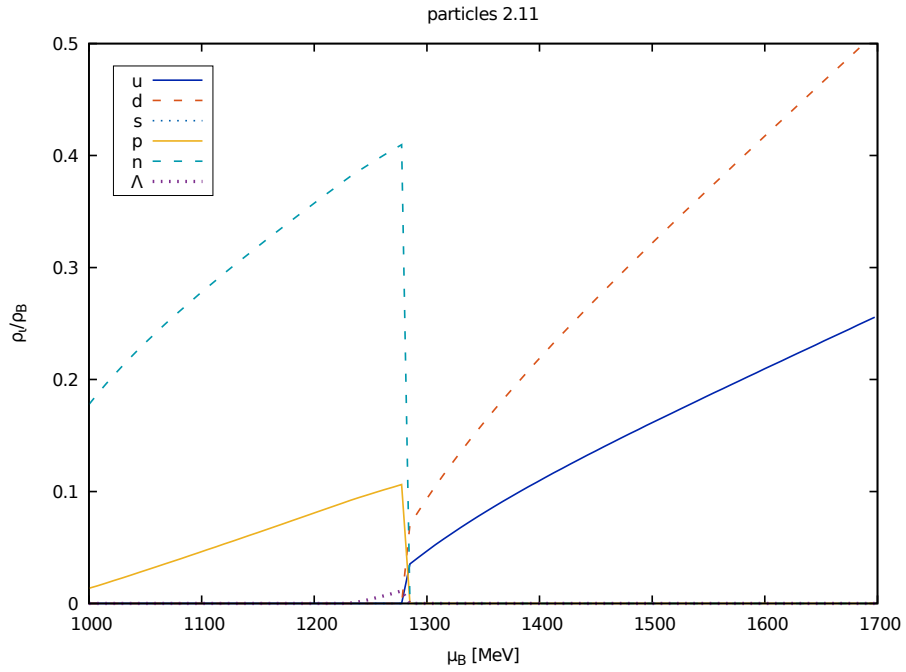

Figure 20: Particle densities (see t1.5 in table 1)

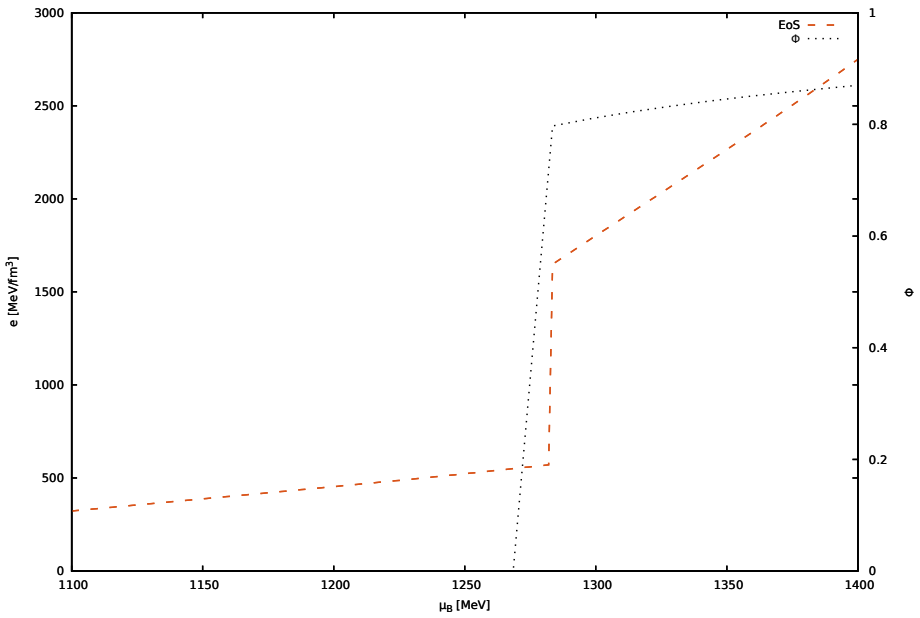

Figure 21: EoS and Polyakov loop (see t1.5 in table 1)

So looking at the different equation of states, one can conclude that the higher the a_1 parameter, the earlier the phase transition occurs. It is not very clear how the parameter of the Polyakov loop influences the particle compositions of the stars either in the hadronic or quark phase. It seems that the amount of protons, neutron and later u and d quarks decreases with increasing a_1 but I can not make a definite conclusion about that.

6.2 VARYING THE g_ω^q - COUPLING CONSTANT

The g_ω^q constant is the quark coupling to the ω-vector mesons. In the following I used different parameters for it while leaving the other couplings fixed. I again calculated the energy gap and the pressure of the phase transition (if there existed one). One will see that the higher the quark interaction, the stiffer the equation of state and therefore the star can support a higher maximum mass. This is due to the fact that a bigger repulsive pressure allows the star to have a higher mass before collapsing due to its gravitational force. In the following section, I will vary g_ω^q, again while keeping the other parameters fixed. There will be three tables, each one has another value for a_1. Starting with the highest one, I decreased a_1 from $3.51 \cdot 10^{-3}$ to $1.17 \cdot 10^{-3}$. The smallest gap in energy density is at $g_\omega^q = 3.51 \cdot 10^{-3}$ with $\Delta\epsilon = 929$ MeV. I used this EoS for calculation of the maximum mass and radius of a star.

Table 2: Varying g_ω^q

	g_σ^q	g_d^q	g_ζ^q	g_ω^q	g_ρ^q	g_Φ^q	a_1	$\Delta\epsilon$[MeVfm^{-3}]	p_{pt}[MeVfm^{-3}]
t2.1	-3	0	-3	4.5	0	0	$3.51 \cdot 10^{-3}$	940	120
t2.2	-3	0	-3	4.7	0	0	$3.51 \cdot 10^{-3}$	929	121
t2.3	-3	0	-3	5.3	0	0	$3.51 \cdot 10^{-3}$	960	124
t2.4	-3	0	-3	8.0	0	0	$3.51 \cdot 10^{-3}$	1373	167

In fig. 22 and 23, the phase transition is at a relatively low chemical potential around 1300 MeV. If one compares to fig. 19, where the same value for a_1 had been chosen but at a higher value for g_ω^q, there is no significant difference in the appearance of the phase transition but the appearance of the Polyakov loop is slightly earlier.

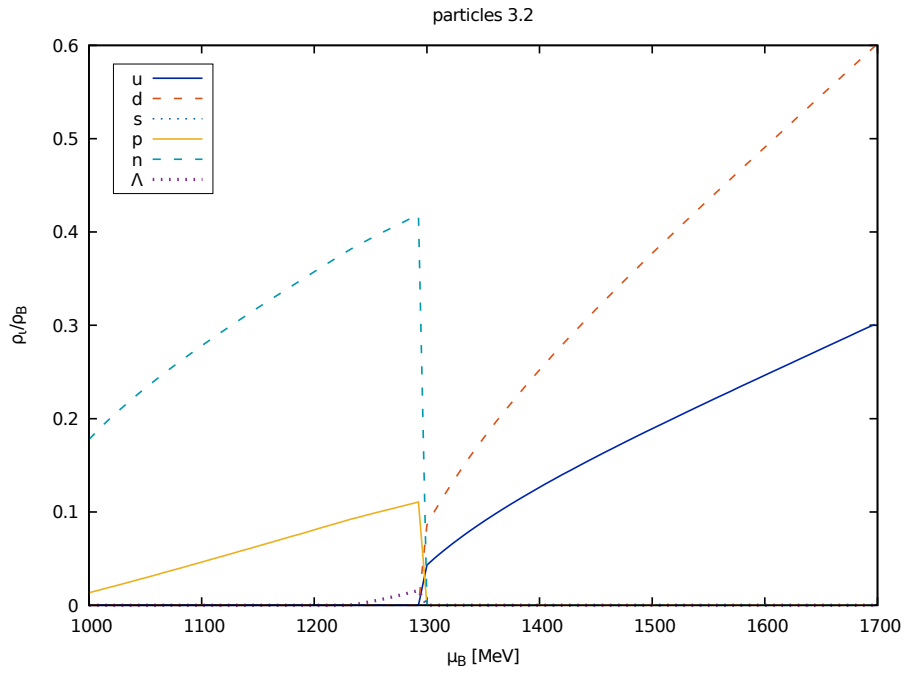

Figure 22: Particle densities (see t2.1 in table 2)

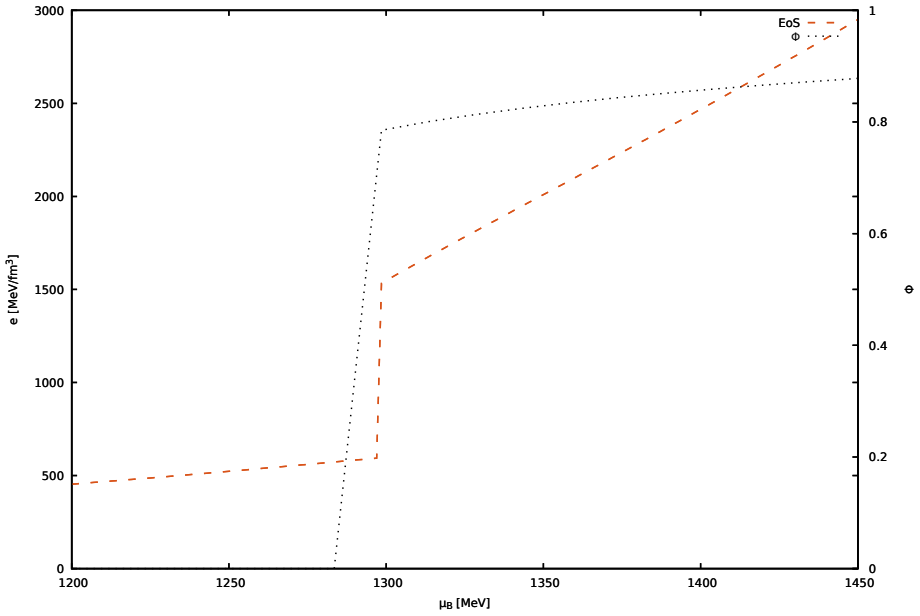

Figure 23: EoS and Polyakov loop (see t2.1 in table 2)

In fig. 24 and 25, g_ω^q is now raised about 0.2. The relative densities of the particles did not change significantly. The occurrence of the phase transition is now a little bit earlier (see pressure in the table), although it is not really visible in the plots. The energy gap is at its lowest now with 929 MeV.

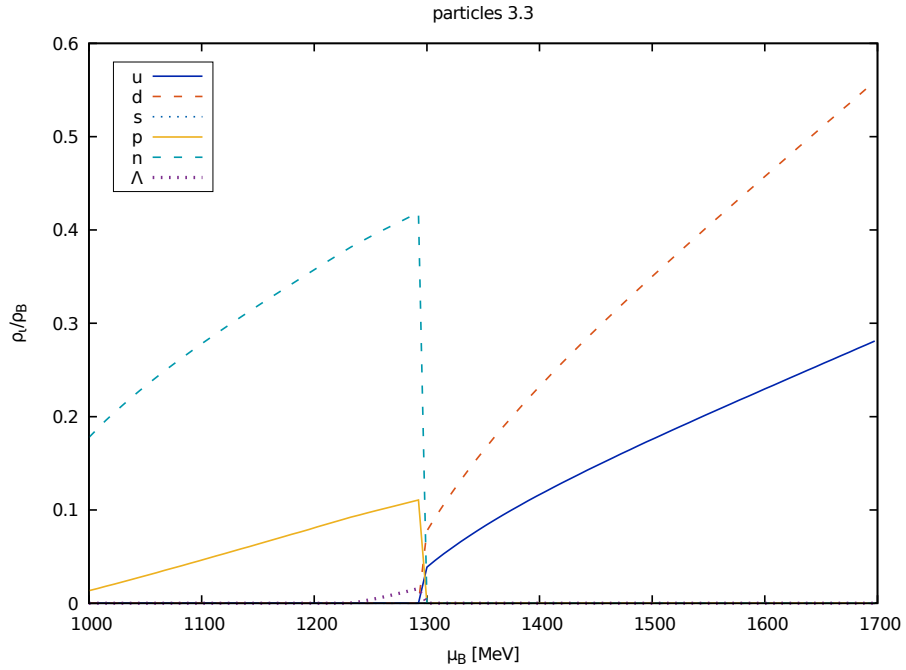

Figure 24: Particle densities (see t2.2 in table 2)

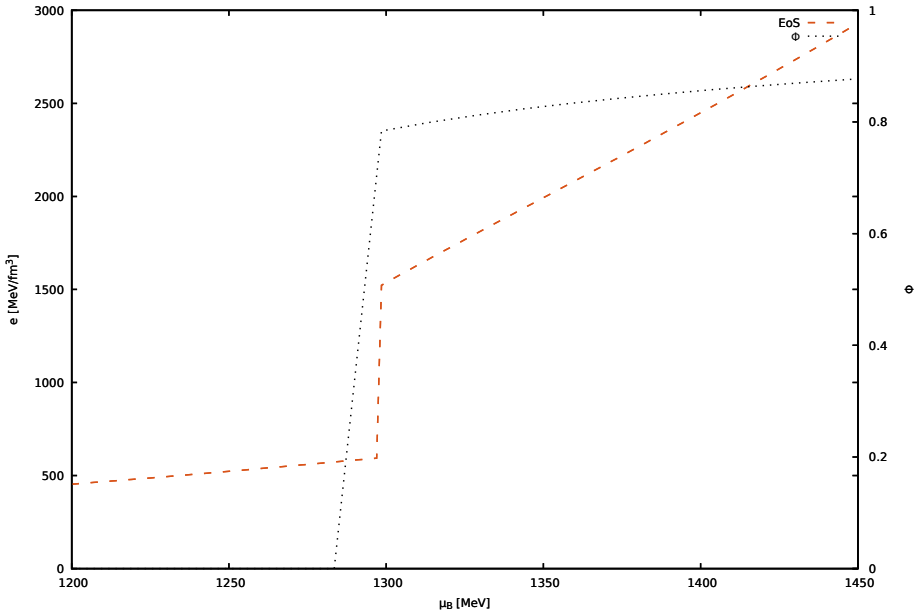

Figure 25: EoS and Polyakov loop (see t2.2 in table 2)

In fig. 26, I used the EoS of fig. 25 for my TOV-solver as it has the smallest gap in energy density and got a maximum mass of $M_{max} = 0.99 M_S$ with a radius of $R_{max} = 7.80$km. The mass did not clearly converge to a constant value because the provided program for the EoS table [8] ended at $\mu_B = 1692$ MeV (this was also true when the upper limit of the loop over the chemical potential was defined at a higher value). The value of the pressure at the phase transition occurs when the curves have a small bend in the EoS table which is seen here at about $r = 4$km.

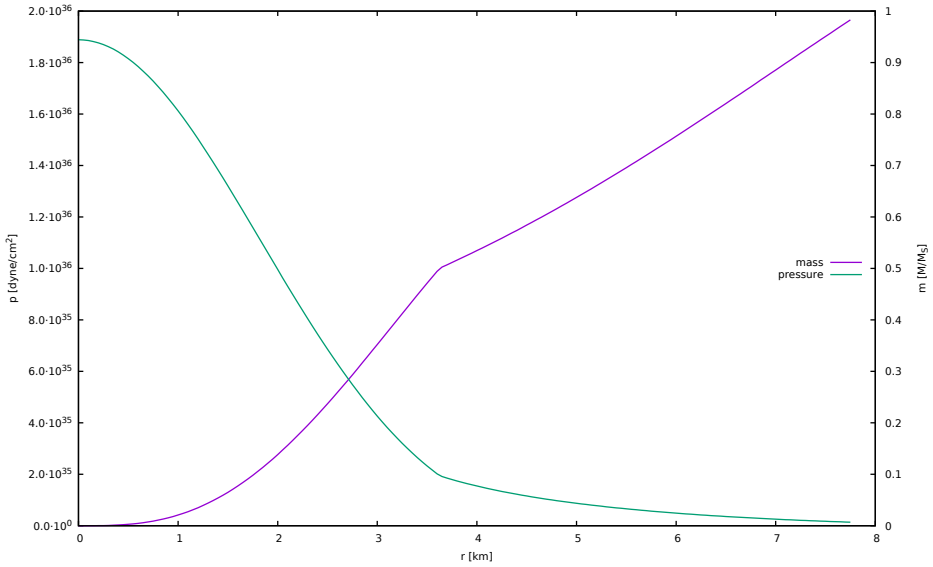

Figure 26: Mass and pressure

In fig. 27 and 28, g^q_ω is now twice as high increased (+0.6). There is no significant change except that the Polyakov loop has a non zero value slightly later than at the previous fig.. The gap in ϵ is raised by 31 MeV.

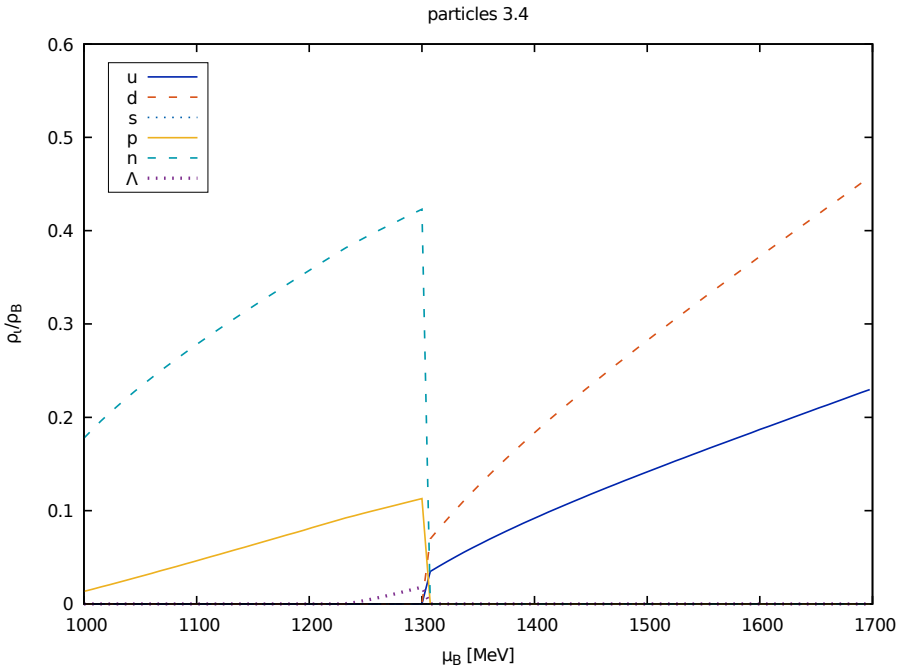

Figure 27: Particle densities (see t2.3 in table 2)

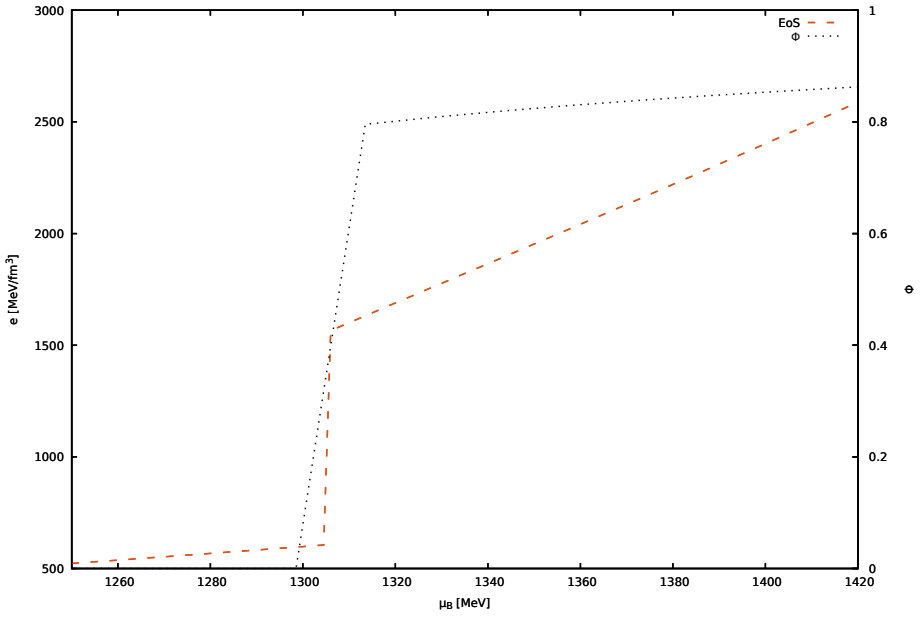

Figure 28: EoS and Polyakov loop (see t2.3 in table 2)

One can see a clear shift in the EoS to a higher chemical potential in fig. 29 and 30, compared to fig. 28. $\Delta\epsilon$ has increased to 1073 MeVfm^{-3}.

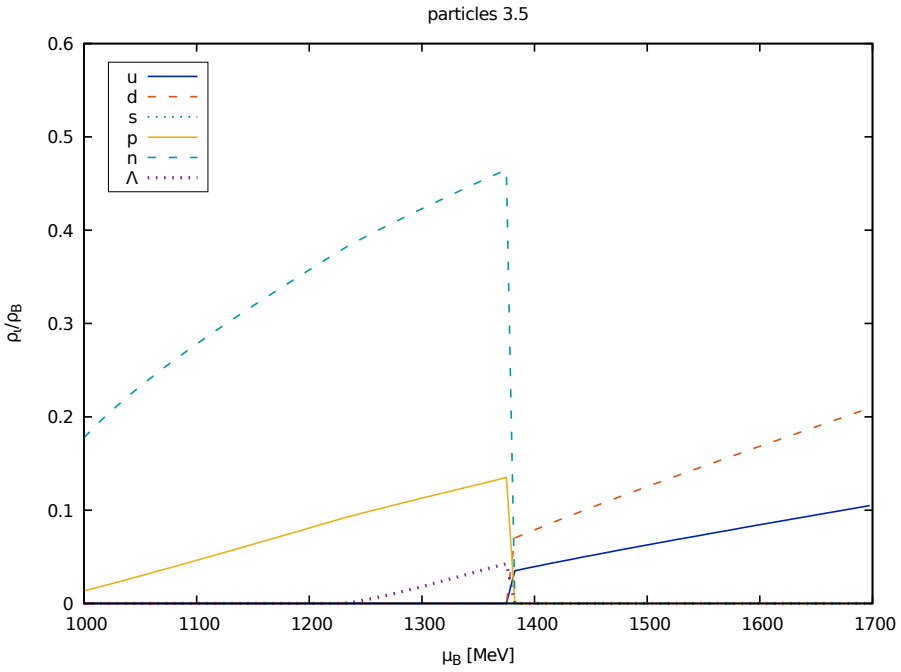

Figure 29: Particle densities (see t2.4 in table 2)

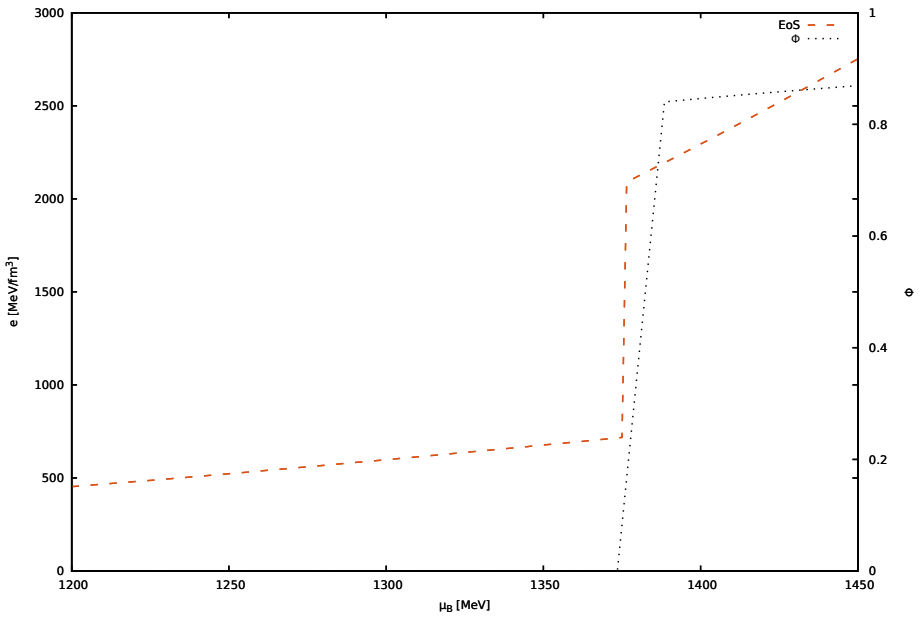

Figure 30: EoS and Polyakov loop (see t2.4 in table 2)

Summarizing it seems that raising the quark coupling g_ω^q leads to a later phase transition. At about $g_\omega^q = 4.7$ there is a minimum in $\Delta\epsilon = 929$ MeV. For the following table I again varied g_ω^q but with a smaller value for a_1. Again, one will see that increasing the value of the quark coupling constant leads to a later phase transition. It is also noticeable how the quark coupling affects the quark density in the quark phase. Also Σ_--baryons will occur in the hadronic phase.

Table 3: Varying g^q_ω

	g^q_σ	g^q_d	g^q_ζ	g^q_ω	g^q_ρ	g^q_Φ	a_1	$\Delta\epsilon$[MeVfm^{-3}]	p_{pt}[MeVfm^{-3}]
t3.1	-3	0	-3	3.0	0	0	$2.886 \cdot 10^{-3}$	1344	177
t3.2	-3	0	-3	4.0	0	0	$2.886 \cdot 10^{-3}$	1265	185
t3.3	-3	0	-3	5.0	0	0	$2.886 \cdot 10^{-3}$	1208	190

The u quarks in fig. 31 have a relative density of $\rho_u/\rho_B = 0.4$ which is approximately as high as the relative neutron density. Interesting at about 1750 MeV is the appearance of s quarks.

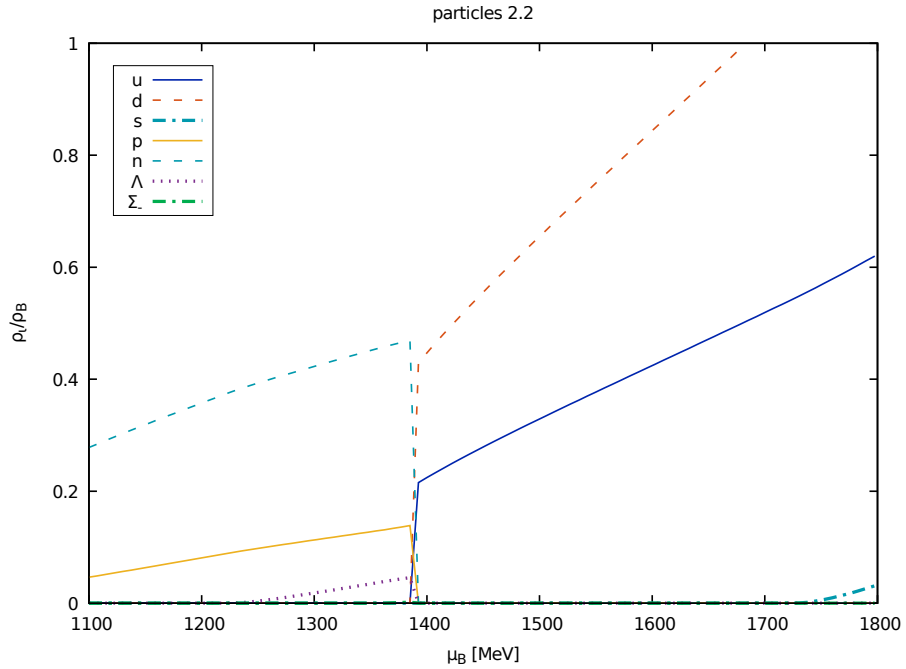

Figure 31: Particle densities (see t3.1 in table 3)

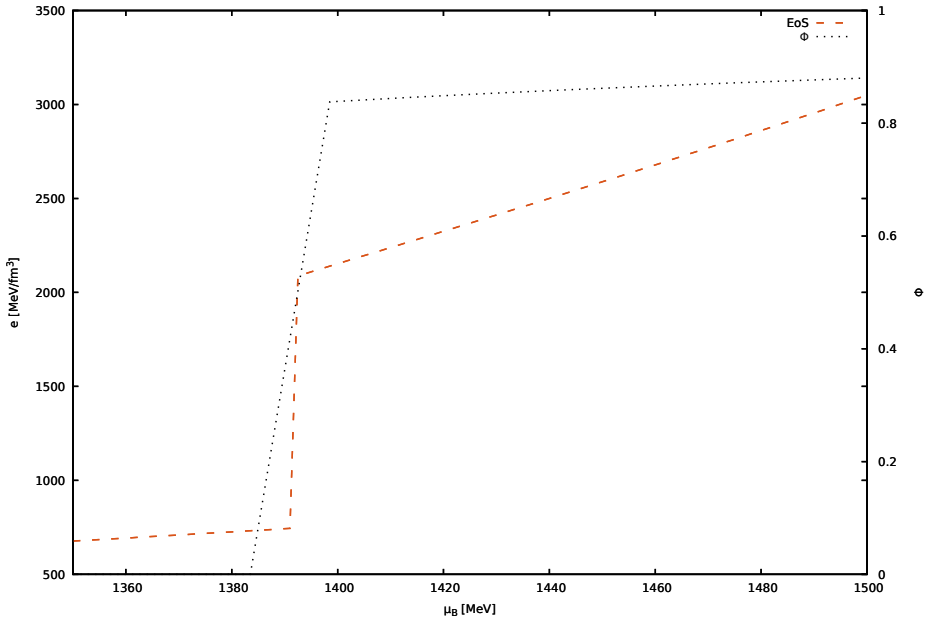

Figure 32: EoS and Polyakov loop (see t3.1 in table 3)

As expected, the phase transition in 34 is at a higher chemical potential. There is a decrease in the u and d quark density in fig. 33. Also Σ_-- baryons shortly appear in the hadronic phase which compose of of two *down* and one s quark. Fig. 37 shows it appearance at around 1400 MeV more detailed.

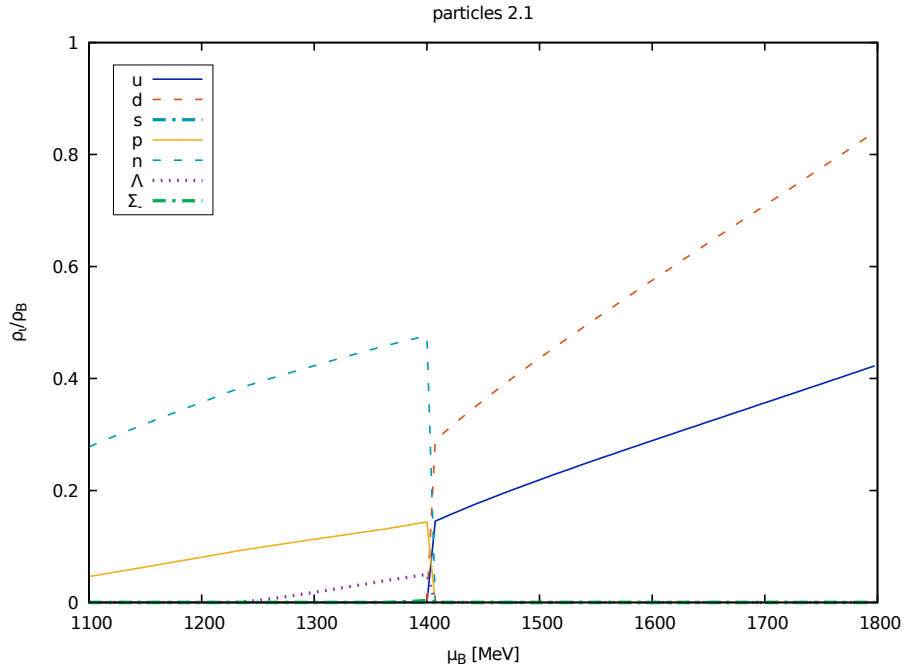

Figure 33: Particle densities (see t3.2 in table 3)

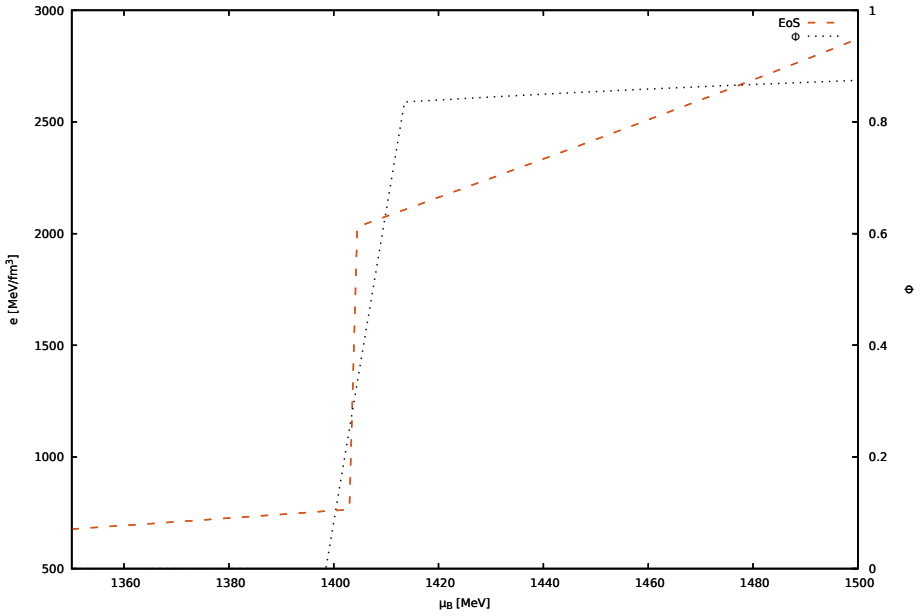

Figure 34: EoS and Polyakov loop (see t3.2 in table 3)

The phase transition in fig. 35 is furthermore shifted to the right to around 1410 MeV fm^{-3}. The density of the quarks (fig. 36) is again decreasing. The Σ_-- baryons again shortly peak at about 1418 MeV (more detailed in fig. 38.)

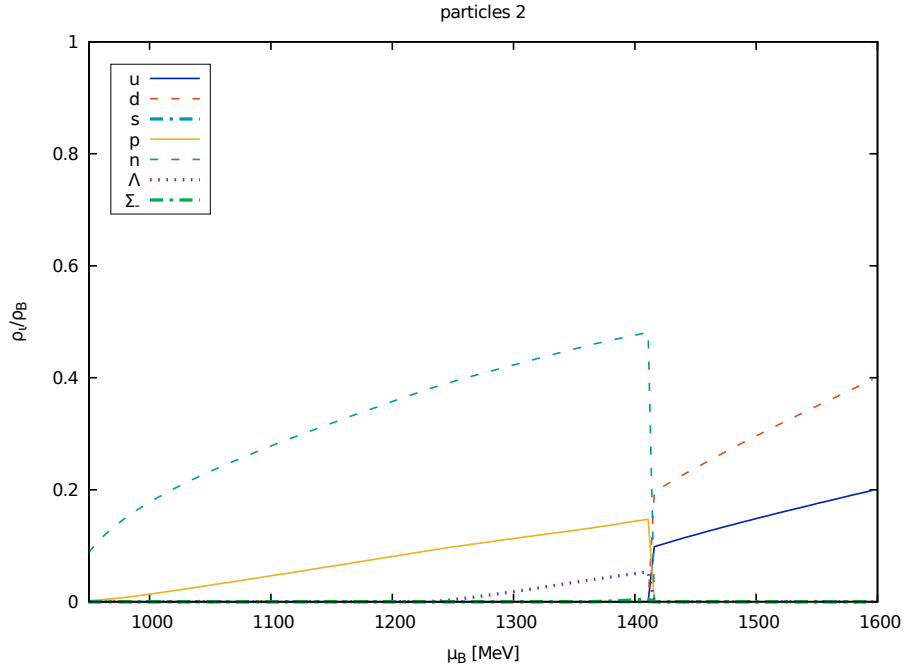

Figure 35: Particle densities (see t3.3 in table 3)

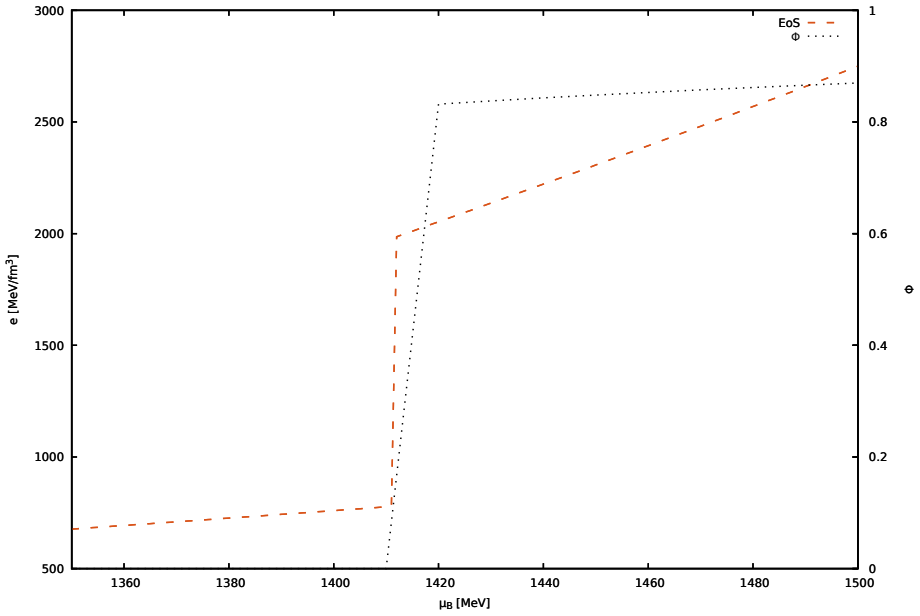

Figure 36: EoS and Polyakov loop (see t3.3 in table 3)

Fig. 37 shows 33 in a more zoomed view. The peak of the Σ_-- baryon lies below 0.005 ρ_{Σ_-}/ρ_B.

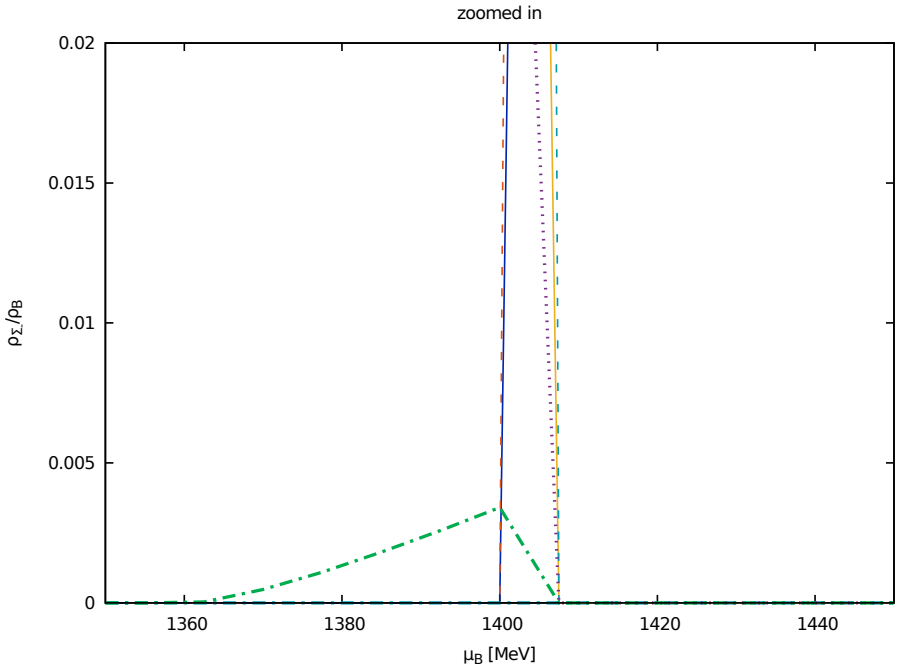

Figure 37: Σ_-- baryon zoomed in (of fig. 33)

The following plot shows a zoomed in version of fig. 35. The peak has a higher peak here at 0.005 ρ_{Σ_-}/ρ_B.

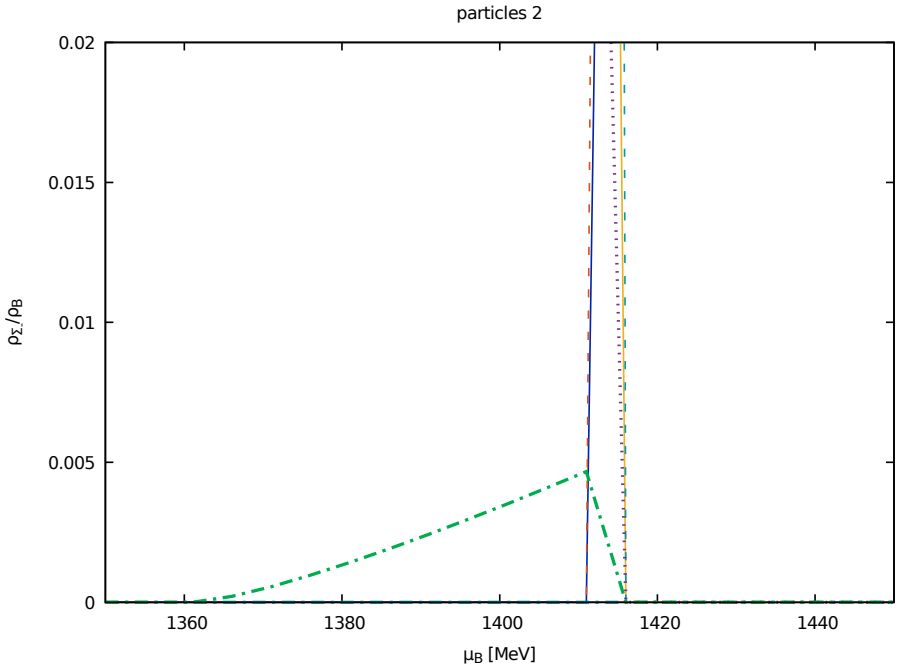

Figure 38: Σ_-- baryon (see fig. 35)

By increasing g^q_ω, the phase transition occurs at a higher chemical potential. Also the relative densities of the u and d quarks are influenced by it. By increasing g^q_ω the densities decrease. At a high enough value for the coupling constant heavier baryons like the Σ_--baryon appear in the hadronic phase.

6.3 SECOND ORDER PHASE TRANSITION

With the following coupling constants I found a second order phase transition which has no latent heat thus no gap in the energy density $\Delta\epsilon$ as function of the chemical potential μ_B. The parameters of table 4 are used.

Table 4: Coupling constants for second order phase transition

g^q_σ	g^q_d	g^q_ζ	g^q_ω	g^q_ρ	g^q_Φ	a_1
-3	0	-3	1.0	0	0	$5.77 \cdot 10^{-4}$

In fig. 39, the y-axis is plotted at log-scale in particle densities. In the hadronic phase, neutrons, protons, Λ- Baryons and Σ_--Baryons occur at different stages of μ_B. In the quark phase, *down* quarks appear at around 1650 MeV, at around 1950 MeV, u quarks show up and at around 2100 MeV, the heavier s quarks appear.

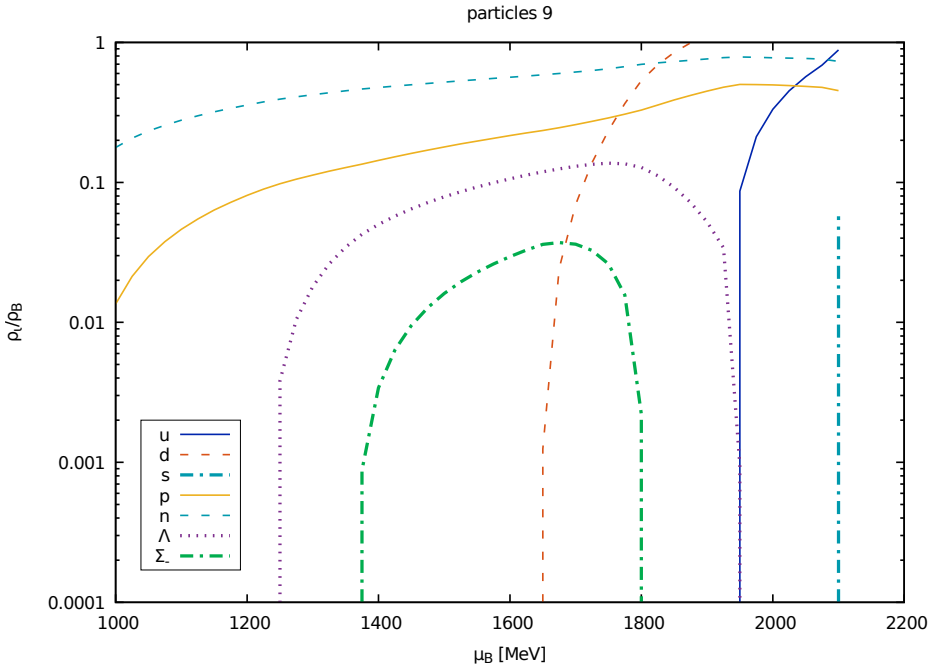

Figure 39: Particle densities plotted on a log scale

There is no energy gap in the phase transition of the EoS in 40. When the Polyakov loop appears at around 1700 MeV, it continuously increases up to 0.5.

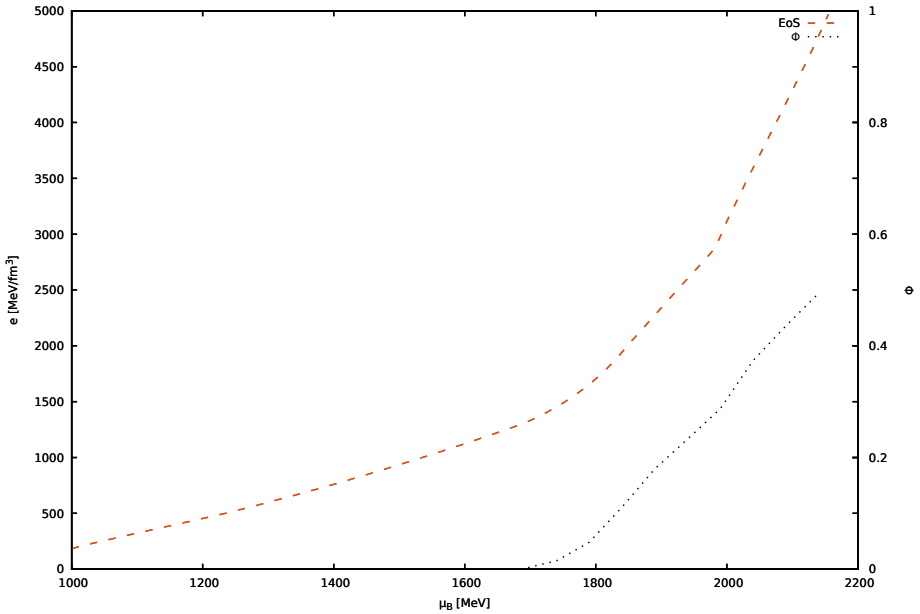

Figure 40: EoS and Polyakov loop

6.4 VARYING THE QUARK MASSES

In the following, I varied the bare masses of the quarks. The coupling constants have been fixed as followed:

Table 5: Coupling parameters

g_σ^q	g_d^q	g_ζ^q	g_ω^q	g_ρ^q	g_Φ^q	a_1
-3	0	-3	5.0	0	0	$3.51 \cdot 10^{-3}$

As one can see in fig. 41, different quark masses influence when the phase transition occurs. On the upper left side the masses of the u and d quarks are indicating the flavor of the corresponding EoS. The s quark its mass is obtained by adding 150 MeV. The heavier the quarks, the later the phase transition.

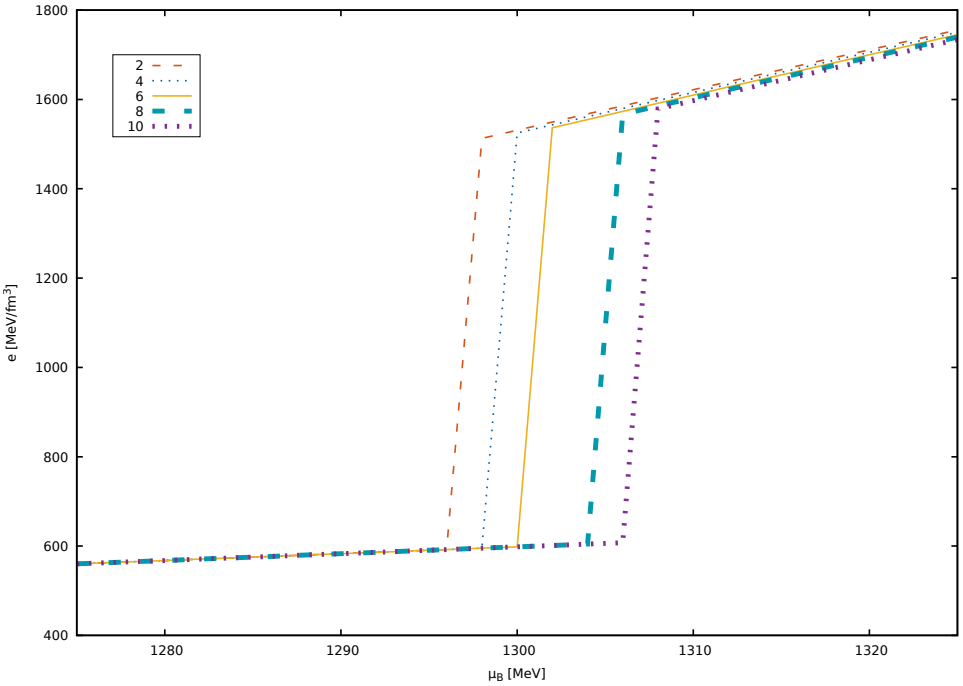

Figure 41: Energy gap in dependence of the quark masses

Varying the mass of the quarks and calculating the gap in the energy densities one gets a clear minimum at about 2.23 MeV for the mass of the u and d quark. The mass of the s quark is obtained by adding 150 MeV.

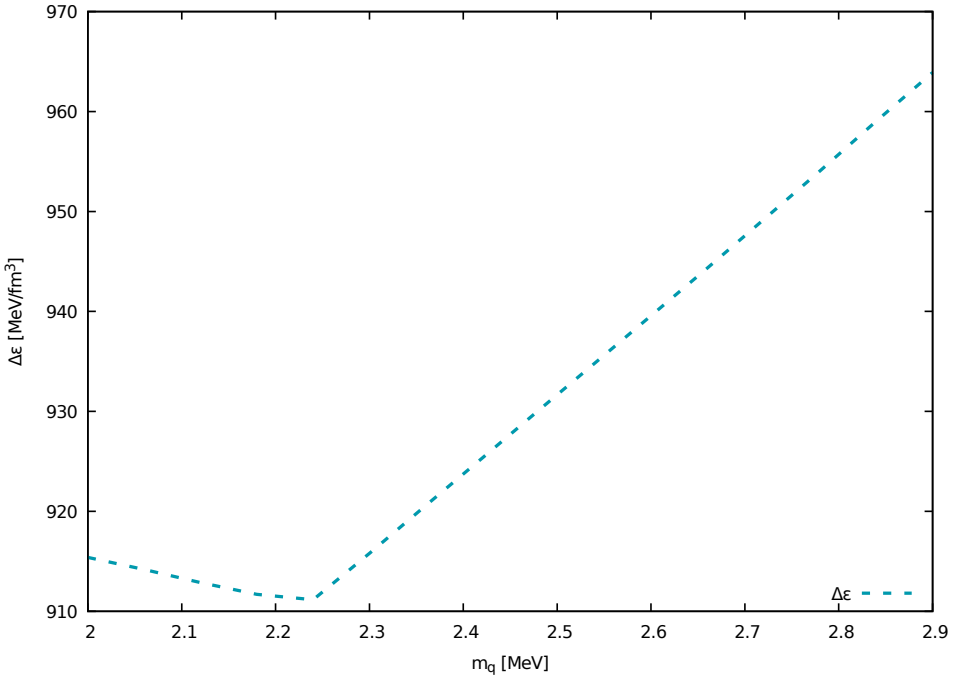

Figure 42: Gap in energy density in dependence of mass of u and d quark

6.5 CONCLUSION

The different EoS that have been discussed have mostly first order phase transitions. The gap in energy density was relatively high with values larger than 900 MeV. A sudden increase in energy density at a fixed value for the pressure leads to an unstable condition for the neutron star. The reason is that the gravitational pressure then starts to dominate the degenerate pressure and the star collapses. Strange quarks in the deconfined phase did occur in two cases (fig. 31 and 39) where a relatively small g_ω^q coupling constant has been chosen. In the hadronic phase (see fig. 33/37 and 35)/38, strangeness occurs in form of of Σ_- baryons. Regarding the various EoS with different parameters (as listed in the tables), I came to the following conclusions for the occurrence of the phase transition as a function if the chemical potential and how the values for a_1, g_ω^q and the quark masses m_q influence the single particles densities.

- increase $a_1 \rightarrow$ earlier phase transition, eventually decrease of neutrons, protons and in the quark phase u and d quarks
- increase $g_\omega^q \rightarrow$ later phase transition, lower density of u and d quarks, also at small values, s quarks did appear
- increase $m_q \rightarrow$ later phase transition

7

IMPLEMENTATION

The following chapter describe the program flow of my implementation. As one can see, the program reads a table from a file (here the EoS-table) and takes these values for its further calculations.

7.1 NO EXTERNAL EOS-TABLE

The first version of my program contained no external tables. The values had been calculated via a formula, the polytropic equation of state and later the Skyrme parametrization, so that the program was very simple. In the file `parameter.f90` the boundary conditions (pressure and mass inside the star at $r = 0$) are set to initial values. They are called p_0 and M_0, M_0 is set to zero while p_0 has a specific value depending on the star. Also all constants and conversion factors between units are defined here.
The `eos.f90` calculates the energy density ϵ for a given pressure. The values for ϵ and p are then inserted into the TOV-equations. The TOV-equations are two ordinary differential equations which can be solved with different methods. I will discuss one of them, the Euler method, in the next section.
As shown in the graph $p(r_{i+1})$ and $M(r_{i+1})$ are calculated in each step in the `rk.f90`-file. Because the radius is increasing, the pressure at the position r_i decreases. Theoretically the loop over the radius should stop when the surface of the star is reached. In practice p never became zero (in my implementation). For that reason I checked for the value of p falling below a certain value or became NaN. If that was the case, the latest calculated mass and its radius where written in the file `p_loop.p` (this is the "no"-branch in diagram 43). Subsequently the starting pressure is varied and the programs over with these new parameters.
In case the surface of the star has not been reached yet, the loop continues, the values $p_(r_{i+1})$, $M_(r_{i+1})$ and R_{i+1} are written into the file `pressure_mass.csv` and the energy density at the new position is calculated. The main methods only coordinates the program flow and loops over the radius R and the outer loop over the starting pressure p_0. Following a summary over the single modules and its functions/parameters:

`parameter.f90`
In this module all constants are defined. Since I am using different units (CGS-units, natural and geometrized units) in different calculations to avoid under or overflow errors, the conversion from one unit into another take place here. All natural constants are defined in CGS-units from which they are converted into geometrized units. Also initial staring values (pressure and mass) are defined here.

`eos.f90`
The two equation of states (Polytropic and Skyrme parametrized) that I used are defined here as a function. For more complex EoS this file instead reads a table with values.

`ode.f90`
Here the TOV-equations are defined. Therefore the derivatives of pressure and mass are needed. These equations are then solved in the `rk.f90` file.

`rk.f90`
Here the ODE solvers are implemented. With the Runge-Kutta or Euler method, one obtains the pressure and mass at at the new position $R_i + \Delta r$.

`main.f90`
The main file retrieves the input from the user, e.g. which unit to choose. Also a loop over the radius R with an initial step size h (defined in `parameter.f90`) is implemented here as well as an outer loop over the starting pressure p_0.

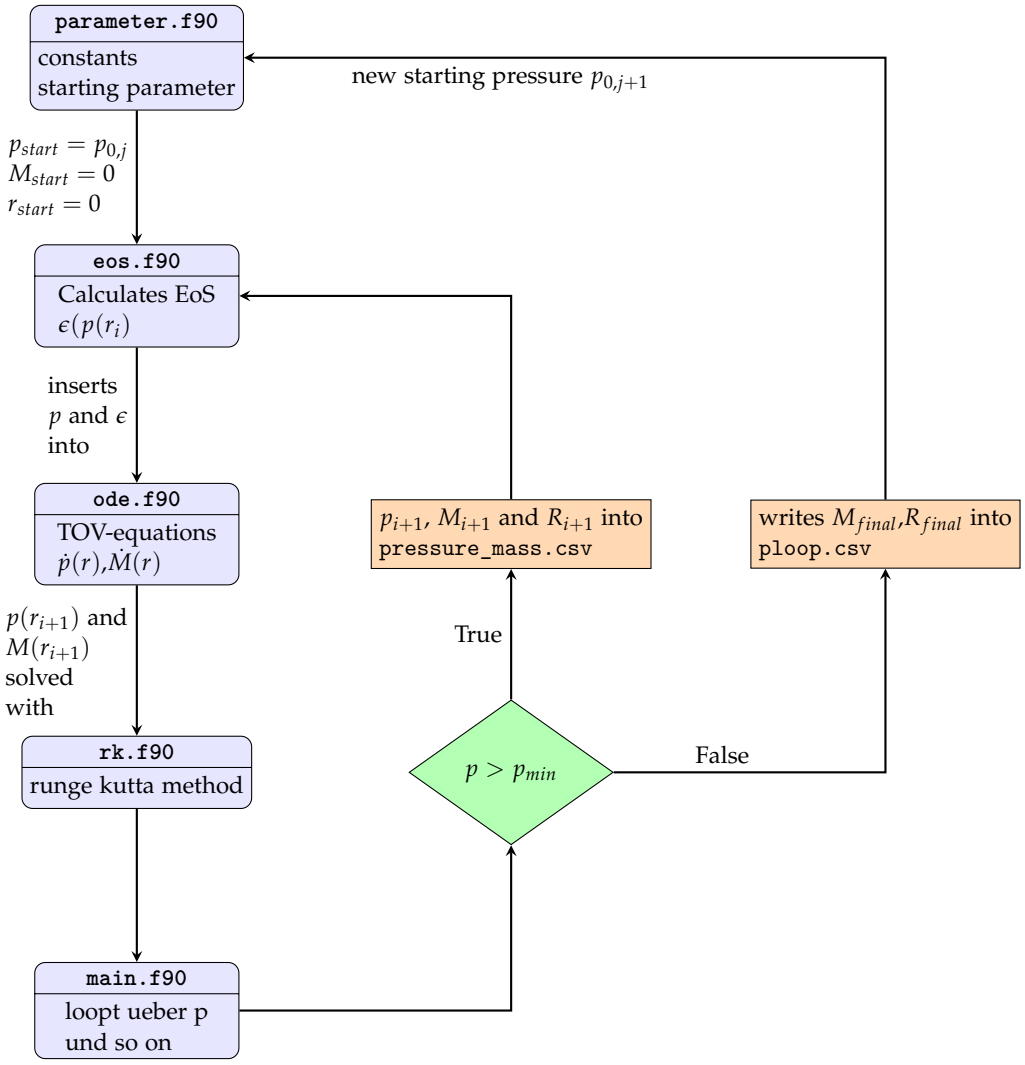

Figure 43: Program flow with EoS derived from given formula

7.2 EXTERNAL EOS

Reading in the file `table.f90` changes the structure of the code bit. It is necessary to define a function which finds the nearest value in a list given the current state of the program. The values of the table that I received had been sorted (if not it can be sorted in $\mathcal{O}(N\log(N))$, with N being the length of the list [7]). One begins with a starting pressure p. The table contains all values of the pressure p_i and the energy density ϵ_i, so that a method is required which finds the value for p with the smallest difference $p_i - p$, where p_i is the i'th element of the list (and the corresponding energy density ϵ).
I implemented both linear (with a runtime of $\mathcal{O}(n)$) and binary search (runtime of $\mathcal{O}(log(n))$) in order to allow scaling to large tables i.e. more precise calculations.
Since the tables in my cases only had about 1000 entries, the linear search had a very short runtime and turned out to be faster than the binary search. The reason was that the searched entries mostly lay at the beginning or ending of the list (depending weather the pressure was de- or increasing with increasing row index) and the asymptotic advantage of be binary search could not overcome the additional constant factor. That was the case because I chose a step size h in the Runge Kutta method, so that the calculated pressure at the next position lay in the same step size range as the pressure $p_{i+1} - p_i$ in the file. Everything else would be wasting information about the table by jumping entries in the table (but it would neither have an advantage in precision taking a step size which leads so smaller steps in Δp than in the table $p_{i+1} - p_i$).
So starting the linear search at the "right" end (which is easily figured out by checking the table), was very effective. This accounts for the disadvantage of the binary search which has its maximum runtime if the searched entries lie at the corners of the table as it needs to "fold" many times.
Instead of starting the linear search always again from the first element (or the last, depending on the order) of the table, I chose as a staring value the latest p_i which was found with the linear search a step earlier since the searched pressure was increasing linear.
Since the linear search only finds the "nearest" value for a given value for p, it is necessary to interpolate the value of the energy density ϵ_{int}. This can be done with the simple linear interpolation, which is really similar to the Euler method (in fact, it is the Euler method in its first step, with $p - p_i$ step size, which ins this case not chosen to be as small as possible but depending on the distance of the "real" pressure p and its nearest table value p_i).
I also implemented a spline interpolation to allow for better scaling to oscillating values of the EoS and better precision in general. Again the advantage turned out to be negligible.
In addition it was necessary to extend the range of values from the EoS table. In order to to this I wrote a fitting function. For low values of the pressure the energy density seemed to have square root like behaviour. Therefore I chose a root function and as quick approximation a linear function as fitting functions. Again the linear approximation turned out to be sufficient. For almost all cases it even turned out to be enough just taking the nearest (last) value in the table. The reason is probably that these regions of the EoS don't contribute much to the overall calculation. In the graph, a more abstract and less detailed flow of the program is presented. It is mainly the same as in the above except for `eos.f90` which changed its interaction in `main.f90`.

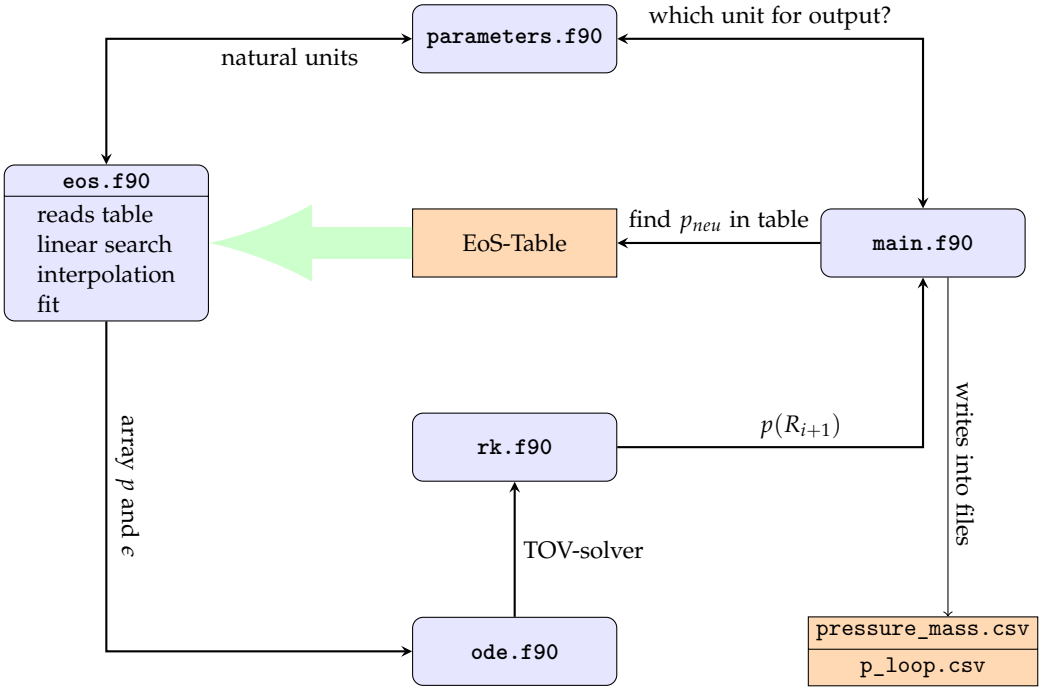

EoS table
Table with parameters for pressure and energy density
eos.f90
This file reads the EoS table. It has the following functions:
`read_table`:
Reads the file and captures the parameters for pressure p and energy density ϵ in two arrays with the dimension of the table
`binary_search/linear_search` :
Finds the next parameter for p and ϵ in the EoS table. The linear search is often faster than the binary search for small table sizes such e.g. 1000 entries. Binary search is useful for big tables but slows down if the searched entry lies at the beginning or ending of the table [7].
`interpolation`:
Since the exact value of the pressure is not given in the table, this function computes interpolation of the data points from the EoS table.

`fit`:
Extrapolated values from the EoS file to small values for the pressure and its corresponding energy density. I used a simple linear function and a root function for extrapolation to small values for p. There where no significant differences in the maximum radii and masses so this function was not used.
Makefiles
Also part of the code where several Makefiles which compile all files and bind them to the program. They also remove auxiliary files.

```
FC = gfortran
FCFLAGS = -Ofast -pg
OBJECTS = main.o ode.o eos.o \
            rk.o parameter.o
%.o: %.f90
$(FC) -c $(FCFLAGS) $<
release: $(OBJECTS)
$(FC) -o main $(FCFLAGS) $(OBJECTS)
clean:
rm -f *.o pressure_mass.csv \
            p_loop.csv fit.csv
```

7.3 UNITS

The natural constants for General relativity and quantum field theory vary in many orders of magnitude. This presents a problem for numerical algorithms. For the polytropic EoS I chose geometrized units. This unit system is helpful because equations like the TOV-equations are better suited for numerical stability with c and G equalling 1. In this unit

system, mass, length, time, energy and momentum are expressed in length (m) and a time interval can be interpreted as the distance light travels in this time.
The main reason why these considerations are important is that computers can only save a finite amount of bits for the representation of a floating point number. The IEEE standard prescribes the following form of floating point numbers

$$x = m \cdot b^e$$

where x is the output number of the computer, m the mantissa and e the exponent. Therefore the number is discretized with increasing gaps for larger exponents. Specifically this results in cancellation of small numbers during subtraction or addition of large numbers. For example an exact subtraction $2.6489789 \cdot 10^{80} - 2.6489100^{80}$ that is represented by the computer in a finite-precision arithmetic $2.6489 \cdot 10^{80} - 2.6489 \cdot 10^{80}$. The mantissa is "cut" because many bits need to be "used up" for the exponent and the result is real equal zero. Therefore it is important for numerical algorithms to use unit systems in which exponents of constants and other values do not get too large. Further details can be found here [26], [18]. Common used constants are

name	symbol	value
speed of light	c	$2.99979 \cdot 10^{8}\mathrm{ms}^{-1}$
Newton's constant	G	$6.6743 \cdot 10^{-11}\mathrm{m}^3\mathrm{kg}^{-1}\mathrm{s}^{-2}$
Planck's constant	$\hbar$	$1.054571726 \cdot 10^{-34}\mathrm{Js}$
Boltzmann constant	k_B	$1.3806488 \cdot 10^{-23}\mathrm{JK}^{-1}$

The units system that I used for studying the EoS derived by the non linear sigma model is the one that is widely used in particle physics, the natural system. Here c, G, the Boltzmann constant $k_B = 1.3806 \cdot 10^{-23}\mathrm{JK}^{-1}$ and the electric constant $\epsilon_0 = 8.8542 \cdot 10^{-12}\mathrm{A}^2\mathrm{s}^4\mathrm{kg}^{-1}\mathrm{m}^{-3}$ are set to 1. Between these units one can further obtain different units by multiplying with the relation $\hbar c = 197.327\mathrm{MeVfm}$ and obtain for energy density and pressure (which have the same units in the natural system) $[\mathrm{MeV}^4]$, $[\mathrm{MeV/fm}^3]$. The conversion factors between all units are in the appendix A.4 as an extract of my code.

7.4 ALGORITHMS

7.4.1 *Euler method*

The implicit Euler-method is a solution method for ordinary differential equations (short: ODE-solver). Given an initial value problem

$$y'(x) = f(x, y(x)) \quad y(x_0) = y_0 \in \mathbb{R}$$

The derivative is defined by the differential quotient with the analytic solution y

$$y'(x) = \lim_{h \to 0} \frac{y(x+h) - y(x)}{h}$$

One can approximate the derivative with the first order term of the Taylor expansion

$$y'(x) = \frac{y(x+h) - y(x)}{h} + \mathcal{O}(h) \simeq \frac{y(x+h) - y(x)}{h}$$

Then one approximates the differential equation $y'(x, y(x))$ with the difference equation

$$\frac{u(x+h) - u(x)}{h} = f(x, u(x))$$

the solution $u(x)$ is then given by

$$u(x+h) = u(x) + hf(x, u(x))$$

For n steps, the iteration towards the $n+1$ step is given by

$$u_{n+1}(x+h) = u(x_n) + hf(x_n, u(x_n)), \quad u(x_0) = y_0$$

Due to the fact that local errors propagate throughout the iteration of the algorithm (as $\mathcal{O}(h)$), error analysis of numerical ode-solvers can become quiet involved.
There are other versions of the Euler method, like the Midpoint method which are more precise. Instead of taking the derivative at a point A, the midpoint method takes the derivative at the point $x/2$ instead at point x. It is also called second order Runge-Kutta method. An n-th order Runge-Kutta method requires n evaluations of the right-hand side per step h. The following graphic illustrates both methods

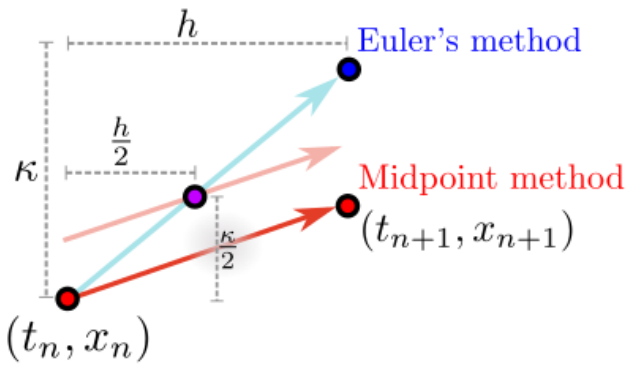

Figure 44: The Euler method goes in the direction of point t_n while the midpoint method goes in the direction of point $\kappa/2$[1]

Detailed derivation as well as considerations regarding local and global errors can be found here [41]. I tested the Euler-method and implemented a fourth order Runge-Kutta-method as well, compared both results and decided to use the Runge-Kutta-method because in my case, the ODE-solver was not critical for the overall runtime but may provide additional stability (although both solvers did not have a significant difference).

7.4.2 *Linear and binary search*

The easiest method to find an element in a sorted list is the linear search. As the name suggests, starting from either the top or bottom of the file, it walks linearly through the sorted list and compares if the current element p_{table} is bigger or smaller than the given value p. As soon as $p_{\text{table}} - p$ changes its sign, the element has been found. Given a large list, the runtime can be long ($\mathcal{O}(N)$) compared to other methods like the binary search for example.
This method takes the middle element of the list and compares if it is smaller or bigger than the element one searches for. The worst-case runtime here is $\mathcal{O}(\log(N))$ for sorted lists. The reason is that, if one bisects a list x-times until it contains only one element, its number of elements is $N = 2^x$. x is obviously the runtime. Solving for x then yields the logarithmic runtime scale.

[1] `www.calculus.seas.upenn.edu`

7.4.3 *Interpolation*

For discretized data points like it is the case for pressure and energy density in the EoS table an interpolation i.e. a method to approximate values in between two data points is necessary. In my case, the Runge Kutta method approximates a solution to the differential TOV- equation i.e. a value for the pressure. The energy density ϵ needs to be interpolated to "fit" it to the value of p. The easiest way to do this is the linear interpolation which also has a quite large error. Let p be the calculated value for the pressure and p_i and p_{i+1} its nearest values of the table with their corresponding values ϵ_{i+1} and ϵ_i. Then the interpolated value of $\epsilon(p)$ is given by

$$\epsilon_{int} = \epsilon_i + \frac{\epsilon_{i+1} - \epsilon_i}{p_{i+1} - p_i} (p_{i+1} - p)$$

The linear interpolation fits the zeroth derivative (the function y itself) with a linear function $y = a_i + b_i x$ on an interval of neighbouring data points $(x_i, y_i), ..., (x_{i+1}, y_{i+1})$ but ignores smoothness of the different lines drawn through the points.
The spline interpolation is more precise. Instead of using a linear connection between the dots one uses a polynomial fit. The cubic spline $S(x)$ replaces linear functions between the data points by degree 3 polynomials. For example if one has n data points $(x_1, y_1), ..., (x_n, y_n)$ in an interval and wants to connect them one gets several so called splines $S_i(x)$ that each fit different data points. They are defined by

$$\begin{aligned} S_1(x) &= y_1 + b_1(x - x_1) + c_1(x - x_1)^2 + d_1(x - x_1)^3 \\ S_2(x) &= y_2 + b_2(x - x_2) + c_2(x - x_2)^2 + d_2(x - x_2)^3 \\ &... \\ S_{n-1}(x) &= y_{n-1} + b_{n-1}(x - x_{n-1}) + c_{n-1}(x - x_{n-1}^2 + d_n - 1)(x - x_{n-1}) \end{aligned}$$

To make sure that the different Splines connect in a smooth way, the following conditions must be fulfilled

1. Condition for the spline to fit the data points
   $S_i(x_i) = y_i,\ S_i(x_{i+1}) = y_{i+1}$
2. slope of neighbouring parts of the spline are the same ($\rightarrow$ smooth transition)
   $S'_{i-1}(x_i) = S'_i(x_i)$
3. same with curvature
   $S''_{i-1}(x_i) = S''_i(x_i)$

Considering the unknown parameter y_i, b_i, c_i, d_i and the conditions that have to be met, one has a system of linear equations that has to be solved. More details about how to solve them and further boundary conditions that have to be met can be found here [20].

7.4.4 *Fit function*

The stopping criterion for the TOV-solver is the pressure to get very small or even zero. This happens when the surface of the star is reached. However in the EoS-table the smallest values for the pressure where relatively big compared to the values that I had used as a stopping criterion so I wanted to check if the maximum mass changed by using a fit function in small regions of p and ϵ. I used a root function which intersects at the midpoint (because at zero pressure, the energy density should be zero as well).
Since this did not change the maximum masses for my test calculations I then resorted to the fastest approximation of taking the lowest known value instead.

A

APPENDIX

A.1 NEWTONIAN FORMULATIONS FOR STARS

For compact stars like white dwarf with a lower mass, one can derive the structure equations of mass and pressure by using classical Newtonian mechanics. Newton's law of gravity for a spherical symmetric system is

$$dF = -G\frac{m\,(r)\;\mathrm{d}m}{r^2} \tag{89}$$

With the gravitational constant $G = 6.67408 \cdot 10^{-11}\,\frac{m^3}{kg \cdot s^2}$ and the radial distance r of the the star. The pressure p is defined as

$$\mathrm{d}p = \frac{dF}{A} \tag{90}$$

with $A = \int_A \mathrm{d}A = r^2 \int_0^{\pi} \sin\theta \mathrm{d}\theta \int_0^{2\pi} \mathrm{d}\varphi = 4\pi r^2$ (in spherical coordinates), this leads to

$$\mathrm{d}p = -\frac{Gm(r)\mathrm{d}m}{4\pi r^4} \tag{91}$$

We can rewrite this in therms of the energy density $\epsilon = \rho c^2$, with the speed of light $c = ...$

$$\mathrm{d}m = \rho(r)\mathrm{d}A\mathrm{d}r = 4\pi\rho(r)r^2\mathrm{d}r = \frac{4\pi\epsilon(r)r^2 dr}{c^2} \tag{92}$$

which leads to the mass-radius relation

$$\leftrightarrow \frac{\mathrm{d}m}{\mathrm{d}r} = \frac{4\pi\epsilon\,(r)}{c^2} \tag{93}$$

and with inserting 92 into 91 to the pressure-radius relation

$$\frac{\mathrm{d}p}{\mathrm{d}r} = -\frac{G\pi\epsilon(r)m(r)}{c^2r^2} \tag{94}$$

These two coupled, linear first order differential equations can be solved numerically.

A.2 INTEGRAL FOR POLYTROPIC EOS

$$\epsilon_{elec}(k_F) = \frac{1}{\pi^2\hbar^3}\int_0^{k_F} E(k)k^2\mathrm{d}k \tag{95}$$

$$= \frac{1}{\pi^2\hbar^3}\int_0^{k_F} \sqrt{m_e^2c^4 + k^2c^2}k^2\mathrm{d}k \tag{96}$$

with the substitution $u := \frac{k}{m_ec}$ and $\mathrm{d}k = m_ec\,\mathrm{d}u$, one obtains

$$\epsilon_{elec}(k_F) = \epsilon_0\int_0^{k_F/m_ec} u^2\sqrt{u^2+1}\,\mathrm{d}u, \tag{97}$$

with $\epsilon_0 := \frac{m_e^4 c^5}{\pi^2 \hbar^3}$.. $X := \int \sqrt{u^2+1}\,\mathrm{d}u$ and $x := \frac{k_F}{m_e c}$. The integral can be written (with partial integration) as:

$$I = \epsilon_0 \left[X u^2 \big|_0^x - \int_0^x 2uX \mathring{d}u \right] \tag{98}$$

The first step is solving the integral in X. This is easily done with the substitution $u := \sinh(t)$, $\mathrm{d}u = \mathrm{d}t \cosh(t)$. The following relations of hyperbolic sine and cosines will be used:

$$\begin{aligned}
\cosh^2(t) &= 1 + \sinh^2(t) \\
\cosh(2t) &= \cosh^2(t) + \sinh^2(t) \\
\cosh^2(t) &= \frac{1}{2}(\cosh(2t) + 1) \\
\cosh(2t) &= 2\sinh^2(t) + 1 \\
\sinh(2t) &= 2\sinh(t)\cosh(t) \\
\sinh^{-1}(t) &= \ln\left(t + \sqrt{t^2+1}\right) \\
\sqrt{t^2+1} &= \cosh\left(\sinh^{-1}(t)\right) \\
\frac{\mathrm{d}}{\mathrm{d}t}\sinh^{-1}(t) &= \frac{1}{1+t^2}
\end{aligned}$$

$$\begin{aligned}
X &= \int \mathrm{d}t \cosh(t)\sqrt{\sinh^2(t)+1} = \int \mathrm{d}t \cosh^2(t) \\
&= \frac{1}{2}\int \mathrm{d}t\,(\cosh(2t)+1) \\
&= \frac{1}{2}\left(t + \frac{1}{2}\sinh(2t)\right) = \frac{1}{2}\left(\,t + \sinh(t)\cosh(2t)\right)
\end{aligned}$$

Backsubstitution yields

$$X = \frac{1}{2}(u\sqrt{u^2+1} + \sinh^{-1})$$

So eq. 98 gets

$$I = \epsilon_0 \left[\frac{1}{2}\left(u\sqrt{u^2+1} + \sinh^{-1}(u)\right) u^2 \big|_0^x - \int_0^x \mathrm{d}u \left(u^2\sqrt{u^2+1} + u\sinh^{-1}(u)\right) \right] \tag{99}$$

$$\tag{100}$$

One can now see that the integral reproduces itself

$$\Rightarrow I = \frac{\epsilon_0}{2}\left[\frac{1}{2}\left(u\sqrt{u^2+1} + \sinh^{-1}(u)\right) u^2 \Big|_0^x - \int_0^x \mathrm{d}u\, u \sinh^{-1}(u) \right] \tag{101}$$

so the only integral which is left is the right term

$$\begin{aligned}
Y &:= \int_0^x \mathrm{d}u u \sinh^{-1}(u) \\
&\overset{\text{p.I.}}{=} u \int \mathrm{d}u \sinh^{-1}(u)\Big|_0^x - \int_0^x \left(\int \mathrm{d}u \sinh^{-1}(u)\right)\mathrm{d}u
\end{aligned}$$

This first term can easily be solved again with partial integration

$$\begin{aligned}
\int \mathrm{d}u \sinh^{-1}(u) &= u\sinh^{-1}(t) - \int \mathrm{d}u \frac{u}{\sqrt{u^2+1}} \\
&= u\sinh^{-1}(u) - \sqrt{1+u^2}
\end{aligned}$$

so that one has

$$Y = u[u\sinh^{-1}(u) - \sqrt{1+u^2}]\Big|_0^x - \int_0^x \mathrm{d}u\, u\sinh^{-1}(u) + \int_0^x \mathrm{d}u\sqrt{1+u^2}$$

The last term is X, which I calculated above (eq. 99). The integral again reproduces itself so bringing the second term to the right side and dividing by two yields

$$Y = \frac{1}{4}[2u^2\sinh^{-1}(u) - u\sqrt{1+u^2} + \sinh^{-1}(u)]\Big|_0^x$$

Inserting this into eq. 101 and one obtains for the whole integral after some simple algebra

$$I = \frac{\epsilon_0}{8}[(2u^3+u)(u^2+1)^{1/2} - \sinh^{-1}(u)]\Big|_0^x \tag{102}$$

$$= \frac{\epsilon_0}{8}[(2x^3+x)(x^2+1)^{1/2} - \sinh^{-1}(x)] \tag{103}$$

A.3 CALCULATION OF P(k_F)

The first step is to get an equation for p derived out of ϵ. One starts with the first law of thermodynamics:

$$\epsilon = Ts - p + \sum_0^N \mu_i n_i \tag{104}$$

it follows at constant number of particles in a free electron gas at $T = 0$

$$\epsilon = n\mu - p \tag{105}$$

with the chemical potential of the electrons

$$\frac{\mathrm{d}\epsilon}{\mathrm{d}n_e} = \mu_e, \tag{106}$$

one gets for p

$$p = n\frac{\mathrm{d}\epsilon}{\mathrm{d}n} - \epsilon = n^2\frac{\mathrm{d}((\epsilon/n)}{\mathrm{d}n} - \epsilon \tag{107}$$

One can now easily calculate p by differentiating equation 102: The contribution of the nucleons to the pressure is zero. (see equation 61). With the definition of k_F (equation 60) and the mass density ρ (equation 59) one obtains for the energy density divided by n:

$$\frac{\epsilon_{elec}(k_F)}{n} = \frac{\epsilon_0}{8}\left[An^{-\frac{2}{3}}(1+A^2n^{\frac{2}{3}})^{\frac{1}{2}} + 2A^3(1+A^2n^{\frac{2}{3}})^{\frac{1}{2}} - \frac{1}{n}\sinh^{-1}(An^{\frac{1}{3}})\right] \tag{108}$$

Differentiating this equation with respect to n yields

$$\begin{aligned}\frac{\mathrm{d}}{\mathrm{d}n}\left(\frac{\epsilon_{elec}}{n}\right) = &-\frac{\epsilon_0}{8}\frac{2}{3}An^{-\frac{5}{3}}(1+A^2n^{\frac{2}{3}})^{\frac{1}{2}} \\ &+ \frac{\epsilon_0}{8}\left[\frac{A^3}{3n}(1+A^2n^{\frac{2}{3}})^{-\frac{1}{2}} + \frac{2}{3}A^5n^{-\frac{1}{3}}(1+A^2n^{\frac{2}{3}})^{-\frac{1}{2}}\right] \\ &+ \frac{\epsilon_0}{8}\left[\frac{1}{n^2}\sinh^{-1}(An^{\frac{1}{3}}) - \frac{1}{3}An^{-\frac{5}{3}}\frac{1}{\sqrt{1+x^2}}\right]\end{aligned} \tag{109}$$

Multiplying with n^2 and replacing $An^{\frac{1}{3}}$ with x leads to

$$p(k_F) = \frac{\epsilon_0}{24}\left[-2x(1+x^2)^{\frac{1}{2}} + \frac{x^3+2x^5-x}{\sqrt{1+x^2}} + 3\sinh^{-1}(x)\right] \tag{110}$$

$$= \frac{\epsilon_0}{24}\left[(2x^2-3x)(1+x^2)^{\frac{1}{2}} + 3\sinh^{-1}(x)\right] \tag{111}$$

A.4 UNIT CONVERSION

```
!naturkonstanten im CGS-System
!==============================
real(kr), parameter :: c     = 29979245800.0_kr                      ! [cm/s]
real(kr), parameter :: G     = 6.6740831_kr*10.0_kr**(-8.0_kr)       ! [cm^3 g^-1 s^-2]
real(kr), parameter :: h_bar = 1.05457266_kr*10.0_kr**(-27.0_kr)     ! [erg s]
real(kr), parameter :: m_n   = 1.674927471214_kr*10.0_kr**(-24.0_kr) ! [g]
real(kr), parameter :: m_e   = 9.1093835611_kr*10.0_kr**(-28.0_kr)   ! [g]
real(kr), parameter :: cb    = c**2.0_kr                             ! [cm^2/s^2]
real(kr), parameter :: pi    = 3.14159265359_kr
real(kr), parameter :: M_s   = 1.98892_kr*10.0_kr**33.0_kr           ! [g]


! SKYRME PARAMETRIZATION NATURAL UNITS
!=====================================
real(kr), parameter  :: h_quer_c     = 197.32705_kr     ![MeVfm]
real(kr), parameter  :: n0           = 0.16_kr          ![fm^-3]
!===EINHEIT DER SKYRME GLEICHUNG (natural units)
! -> p = [MeV^4] = eps = [MeV^4]
! [MeV/fm^3] * (hbar c)^3 -> [Mev^4]
!=========================================================================
real(kr),parameter             :: n_start      = 0.0001_kr*n0*(h_quer_c)/&
&**3.0_kr               ![MeV^3]
real(kr), parameter            :: n_ende       = 20.0_kr*n0*(h_quer_c)/&
&**3.0_kr               ![MeV^3]
real(kr), parameter            :: h_barx       = 1.0_kr
real(kr), parameter            :: mn_nu        = 939.5654133_kr          ![MeV]
real, parameter                :: t0           = 1024.1_kr/(197.33_kr/&
&**3.0_kr)              ![1/MeV^2]
real, parameter                :: t3           = 14600.8_kr/(197.33_kr/&
**6.0_kr)                                ![1/MeV^5]

!===UMRECHNUNG ZU [MeV/fm^3], CGS=====
real(kr), parameter  :: eps_mev4tomevfm = 1.0_kr/(h_quer_c**3.0_kr)      ![MeV/fm^3]
!real(kr), parameter :: eps_mev4togcm   = eps_mev4tomevfm * 1.78266567_kr/&
&*10.0_kr**12.0_kr
!=E[J]/c^2 * 1000 --> [g/cm^3]
real(kr),parameter   :: eps_mevfmtogcm  = 1.7826657_kr*10.0_kr**12.0_kr  ! [g/cm^3]
real(kr), parameter  :: eps_mevfmtocgs  = eps_mevfmtogcm * c**2.0_kr     ![erg/cm^3]
real(kr), parameter  :: p_mev4tomevfm   = 1.0_kr/(h_quer_c**3.0_kr)      ![MeV/fm^3]
real(kr), parameter  :: p_mevfmtocgs    = 1.60218_kr*10.0_kr**33.0_kr
real(kr), parameter  :: p_mevfmtogcm    = 1.7826657_kr*10.0_kr**12.0_kr
!=========================================================================

!Multiplikationsfaktoren von geometrischen in CGS-Einheiten
!==========================================================
real(kr), parameter :: c_geomtocgs   = 1.0_kr
real(kr), parameter :: G_geomtocgs   = 1.0_kr
real(kr), parameter :: p_geomtocgs   = c**4.0_kr/G
real(kr), parameter :: eps_geomtocgs = c**4.0_kr/G
real(kr), parameter :: m_geomtocgs   = c**2.0_kr/G
real(kr), parameter :: cb_geomtocgs  = 1.0_kr
real(kr), parameter :: gamma_nr      = 5.0_kr/3.0_kr
real(kr), parameter :: gamma_r       = 4.0_kr/3.0_kr
real(kr), parameter :: gamma_ur      = 1.0_kr
real(kr), parameter :: Knr_geomtocgs = p_geomtocgs/(eps_geomtocgs**gamma_nr)
real(kr), parameter :: Kr_geomtocgs  = p_geomtocgs/(eps_geomtocgs**gamma_r)


!Berechnung der Parameter in geometrized units
!=============================================
real(kr), parameter :: K_gnr    = h_bar**2.0_kr/(15.0_kr*pi**2.0_kr*m_e)/&
&*(((3.0_kr*pi**2.0_kr)/&
&(m_n*c**2.0_kr*2.0_kr))**(gamma_nr))/Knr_geomtocgs
real(kr), parameter :: K_gr     = h_bar*c/(12.0_kr*pi**2.0_kr)*((3.0_kr*pi**2.0_kr)/&
&(2.0_kr*m_n*c**2))**(gamma_r)/(Kr_geomtocgs)
real(kr), parameter :: K_ur     = 1.0_kr
real(kr), parameter :: m_gn     = m_n/m_geomtocgs
real(kr), parameter :: m_ge     = m_e/m_geomtocgs
```

```
real(kr), parameter :: G_g      = 1.0_kr
real(kr), parameter :: c_g      = 1.0_kr
```

BIBLIOGRAPHY

[1] S. Balberg, I. Lichtenstadt, and G. B. Cook. Roles of Hyperons in Neutron Stars.

[2] E. Bertschinger. Symmetry Transformations, the Einstein-Hilbert Action, and Gauge Invariance. 2002.

[3] H. A. Bethe. *Nuclear many-body problem*, volume 103. 1956.

[4] B. W. Carroll and D. A. Ostlie. *An Introduction to Modern Astrophysics (2nd Ed.)*. Pearson Addison-Wesley, 2006.

[5] S. Carroll. *Spacetime and Geometry: An Introduction to General Relativity*. Pearson, 2014.

[6] S. De Boer. Compact Stars as a Laboratory for Nuclear Matter. 2011.

[7] M. J. Denneen and M. C. Wilson. *Introduction to Algorithms, Data Structures and Formal Languages*. 2004.

[8] V. Dexheimer. *Chiral Symmetry Restoration and Deconfinement in Neutron Stars*. PhD thesis, Goethe University, 2009.

[9] V. Dexheimer and S. Schramm. Proto-Neutron and Neutron Stars in a Chiral SU(3) Model. 2008.

[10] V. A. Dexheimer and S. Schramm. Chiral symmetry restoration and deconfinement to quark matter in neutron stars. *Nuclear Physics B - Proceedings Supplements*, 199(1):319–324, 2010.

[11] T. Fließbach. Allgemeine Relativitätstheorie. *The Astrophysical Journal Supplement Series*, 192(2):14, 2012.

[12] A. Franzke and M. Koch. Allgemeine Evolutionsbiologie, 2014.

[13] Fritzsch K. Spin-Strukturen.

[14] D. Giulini and N. Straumann. Das Rätsel der kosmischen Vakuumenergiedichte und die beschleunigte Expansion des Universums.

[15] N. Glendenning. *Compact Stars*. 1997.

[16] W. Greiner and R. K. Gupta. *Heavy Elements and Related New Phenomena*. World Scientific Publishing Company, 6 1999.

[17] M. Guidry. Principle of Equivalence.

[18] I. P. Iii, A. M. D. Athlon, C. Alpha, T. Ieee, F. Point, I. Floating, P. Standard, E. We, E. Example, M. Numbers, and B. For. Floating Point Arithmetic.

[19] N. Kajuri. Strong equivalence principle in polymer quantum mechanics and deformed Heisenberg algebra. *Physical Review D*, 94(8), 2016.

[20] R. L.Burden and J. D. Faires. *Numerical Analysis*. 2011.

[21] R. Lenz. Group Theoretical Methods in Image Processing, 1990.

[22] D. E. Logan. *Many-Body Quantum Theory in Condensed Matter Physics—An Introduction*, volume 38. 2005.

[23] M. Malheiro, S. Ray, and V. T. Zanchin. ELECTRICALLY CHARGED NEUTRON STARS.

[24] X. Mei. The Precise Inner Solutions of Gravity Field Equations of Hollow and Solid Spheres and the Theorem of Singularity. *International Journal of Astronomy and Astrophysics*, 01(03):109–116, 2011.

[25] M. Murthy. High energy physics, Draft notes, 2007.

[26] A. L. Myers. NATURAL SYSTEM OF UNITS IN GENERAL RELATIVITY.

[27] R. Nave. Particle Interactions and Conservation Laws, 2001.

[28] K. Olive and Particle Data Group. Summary of Quark Masses. *Chinese Physics*, 090001(C38):1–3, 2014.

[29] O. Philipsen. Quantenfeldtheorie und das Standardmodell der Teilchenphysik, 2016.

[30] M. Prakash, J. M. Lattimer, J. A. Pons, A. W. Steiner, and S. Reddy. Evolution of a Neutron Star From its Birth to Old Age. 2000.

[31] J. Rafelski. STRANGENESS PRODUCTION IN THE QUARK GLUON PLASMA. 1983.

[32] P. Ring and P. Schuck. *The nuclear many-body problem*, volume Texts and. 1980.

[33] D. H. Rischke. Theoretische Physik VI: Quantenmechanik II, 2016.

[34] I. Sagert, M. Hempel, C. Greiner, and J. Schaffner-Bielich. Compact Stars for Undergraduates. *Eur. J. Phys.*, 27(3):30, 2005.

[35] K. Schmietendorf. Die Gruppe SU(3) und das Quarkmodell, 2008.

[36] A. Sedrakian. Introduction to theoretical Astroparticle Physics.

[37] P. Thyssen and A. Ceulemans. *Shattered Symmetry: From the Eightfold Way to the Periodic Table*. 2015.

[38] L. Van Dommelen. The Hartree-Fock Approximation.

[39] D. Vautherin and D. M. Brink. Hartree-Fock calculations with Skyrme's interaction. *Physics Letters B*, 32(3):149–153, 1970.

[40] T. VORONOV. DIFFERENTIAL GEOMETRY. S. 2009.

[41] WilliamH.Press, SaulA.Teukolsky, and WilliamT.Vetterling. *Numerical Recipes - The Art of Scientific Computing*. Cambridge University Press, 2007.

[42] B. Ziebarth. Relativistische Hydrostatik und die Tolman-Oppenheimer-Volkoff-Gleichung, 2010.

Erklärung nach § 30 (12) Ordnung für den Bachelor- und Masterstudiengang

Hiermit erkläre ich, dass ich die Arbeit selbstständig und ohne Benutzung anderer als der angegebenen Quellen und Hilfsmittel verfasst habe. Alle Stellen der Arbeit, die wörtlich oder sinngemäß aus Veröffentlichungen oder aus anderen fremden Texten entnommen wurden, sind von mir als solche kenntlich gemacht worden. Ferner erkläre ich, dass die Arbeit nicht - auch nicht auszugsweise - für eine andere Prüfung verwendet wurde.

Frankfurt am Main, November 12, 2017

Pia Jakobus